Validation of Satellite Precipitation Estimates over the Western Cape Region, South Africa

JAN DE WAAL,[a] MARLON MARANAN,[b] ANDREAS H. FINK,[b] ANDREW WATSON,[c] ASHWIN BENNETT,[a] AND JÖRG HELMSCHROT[b,c]

[a] *Department of Geography and Environmental Studies, Stellenbosch University, Stellenbosch, South Africa*
[b] *Institute of Meteorology and Climate Research, Karlsruhe Institute of Technology, Karlsruhe, Germany*
[c] *School for Climate Studies, Stellenbosch University, Stellenbosch, South Africa*

(Manuscript received 17 September 2024, in final form 21 January 2025, accepted 3 March 2025)

ABSTRACT: Precipitation gauging networks have been declining in many developing countries such as South Africa. Satellite-based precipitation products (SPPs) and reanalysis data have shown vast improvements over the last 5 years and are postulated to mitigate the lack of ground-based observations. The Western Cape of South Africa has recently experienced a devastating drought (2015–18) and consecutive local floods (2023/24) but lacks sufficient precipitation observations to fully conceptualize the impacts of these climatic extremes. Using a variety of statistical metrics, we analyze the performance of six SPPs and reanalysis-driven datasets, namely, Climate Hazards Group Infrared Precipitation with Stations (CHIRPS V2), ERA5, Multi-Source Weighted-Ensemble Precipitation (MSWEP V2.8), and Integrated Multi-satellitE Retrievals for Global Precipitation Measurement (IMERG) (Early and Final Runs of V6B, Final Run of V7) compared with historical records collected from local weather bureaus from 2012 to 2021. On a daily scale, reanalysis products such as ERA5 and MSWEP outperform other SPPs concerning a dichotomous wet-/dry-day distinction, temporal rainfall pattern, and Heidke skill score. All products performed best in the wet parts of the year (JJA), and performance is influenced by climate zone and topography. All products performed poorly for extreme values (i.e., >95th percentile) and are therefore of less use for evaluating potential flood peaks. SPP performance was more related to climate type as opposed to altitude, and future improvements in SPPs should focus on local microclimatic variability to capture headwater precipitation patterns. While in the African tropics, infrared (IR)/passive microwave (PMW)-based products perform best, in the Mediterranean climate region of the Western Cape, reanalysis-driven products are superior.

SIGNIFICANCE STATEMENT: The use of satellite-based precipitation products (SPPs) and reanalysis data can mitigate the decline in observation stations in many countries, particularly in the Global South. While the performance of SPPs in tropical and subtropical climates in Africa has been previously investigated, this paper is among the first research into the efficacy of SPPs in the Mediterranean climate zone of southern Africa. Results from the research can potentially be extrapolated to other Mediterranean climates globally.

KEYWORDS: Africa; Water resources; Precipitation; Satellite observations; Satellite Precipitation Products

1. Introduction

The measurement of precipitation is of critical importance for water resource management, flood and drought forecasting, and hydrological modeling applications globally (Brunner et al. 2021). The global network of rain gauges (RGs) is, however, unevenly distributed with some regions having relatively high densities of gauges compared to others with sparse coverage (Villarini et al. 2008). In particular, the number of precipitation stations is often congested around urban centers, while station coverage in many rural regions and high-altitude areas, with poor telecommunication, is limited (Chawla and Mujumdar 2020). In Africa, like many regions in the Global South, a trend of decreasing station availability since the 1970s is evident (Nicholson et al. 2018a,b). Not only has this affected the already low spatial density of stations—just one per 26 000 km^2 (Washington et al. 2006)—but also disrupted extensive precipitation time series which are crucial for analyses regarding long-term trends and decadal variability. The latter is highlighted in a pan-African study by Nicholson et al. (2018a) who leveraged up to centennial-long station data to identify changes in the characteristics of agriculturally relevant seasonal rainfall. For hydrological applications on shorter time scales, the irregular distribution of rain gauge networks means that spatial averages contain bias, thereby reducing hydrological model performance (Zeng et al. 2018) and, thus, the flood forecasting capabilities and mapping zones of high flood risk. Likewise, the continuity of data from precipitation stations is important to ensure that temporal biases are not created by a change in station density, especially for climate and hydrological change assessments. South Africa also exhibits a rapid decline in rain gauge coverage due to financial constraints imposed on those governmental organizations responsible for data collection (Hughes 2006; Bailey and Pitman 2015). This reduced coverage has limited the ability of researchers and water managers to fully conceptualize the impacts of extreme events such as a

Denotes content that is immediately available upon publication as open access.

Corresponding author: Jan de Waal, janniedw@sun.ac.za

DOI: 10.1175/JHM-D-24-0123.1

recent severe drought (2015–18) (Wolski 2018) and consecutive local floods (2023/24) (Western Cape Government 2024). As many regions globally are plagued by poor rain gauge coverage, it becomes necessary to assess the emergence of new global datasets and their potential use in hydrological and environmental assessments.

Satellite-based precipitation products (SPPs) provide relatively high temporal and spatial resolution precipitation estimates and can monitor ungauged regions. As such, they offer vast potential for global climate monitoring of the hydrological cycle but naturally suffer from deficiencies due to largely indirect (passive) rainfall retrieval approaches. Satellite-based rainfall estimates can vary considerably due to assumptions regarding the dominant precipitation generation mechanisms, different sensing techniques, and methods used to improve the final data product. The passive estimation of precipitation from remote sensing products falls within two major methodologies (Kidd and Levizzani 2011). The first category leverages the availability of spatiotemporally high-resolution observations (subhourly, a few kilometers at nadir) in the thermal infrared (IR) retrieved from geostationary Earth-orbiting (GEO) satellites. IR-based methods generally convert cloud-top temperature (CTT) information into surface rainfall. Early developments include the GOES precipitation index (Arkin et al. 1994; Arkin and Meisner 1987) which uses a linear relationship between surface rainfall and fractional cloud cover for pixels colder than 235 K. However, modern algorithms involve more complex formulations than this simplistic assumption and often combine CTT information with other rainfall sources. Especially RG observations, commonly retrieved through the Global Telecommunication System (GTS), are harnessed, e.g., within the global dataset Climate Hazards Group Infrared Precipitation with Stations (CHIRPS; Funk et al. 2015), the Africa-focused Tropical Applications of Meteorology Using Satellite Data and ground-based observations (TAMSAT; Tarnavsky et al. 2014), and its derivative TAMSAT African Rainfall Climatology and Time Series (TARCAT; Maidment et al. 2014). Furthermore, artificial neural network (ANN) models have been particularly utilized in the Precipitation Estimation from Remotely Sensed Information Using Artificial Neural Networks (PERSIANN; Hsu et al. 1997) to continuously increase the performance of IR-based rainfall estimations through the incorporation of training datasets such as visible (VIS) imagery and passive microwave (PMW) information from low-Earth-orbiting (LEO) satellites (Nguyen et al. 2018). Most of these IR-based products use RG calibration with gauges like CHIRPS or a climatological CTT-gauge-based relationship like TAMSAT products.

The second category focuses on PMW-based techniques which rely upon a physically more direct relationship between the existence of precipitation-sized particles and subsequent attenuations in the upwelling background microwave (MW) field of Earth (Kidd and Levizzani 2011; Tapiador et al. 2022). PMW methods are frequently combined with IR information to account for observational PMW data gaps. Within the Climate Prediction Center morphing technique (CMORPH; Joyce et al. 2004), IR imagery is used to create cloud motion vectors to "predict" the characteristics and location of PMW rainfall features via spatiotemporal morphing. Combining the capabilities of IR and PMW data in such fashion has found its way into widely used rainfall products, such as the Global Satellite Mapping of Precipitation (GSMaP; Ushio et al. 2003; Kubota et al. 2007), the Tropical Rainfall Measuring Mission (TRMM; Kummerow et al. 2000; Huffman et al. 2007), and its successor Global Precipitation Measurement (GPM; Hou et al. 2014; Huffman et al. 2017). Furthermore, these products are also RG calibrated to account for regional biases and whose methods are inspired by techniques applied in the Global Precipitation Climatology Project (GPCP; Huffman et al. 1997; Adler et al. 2003) using the RG-based products of the Global Precipitation Climatology Centre (GPCC; Schneider et al. 2008). Most recent activities went one step beyond the focus on satellite-based techniques. By blending PMW-based rainfall products with RG observations and reanalysis data from atmospheric models, the Multi-Source Weighted-Ensemble Precipitation (MSWEP; Beck et al. 2017, 2019) was developed to find an optimal merging of data sources as a function of time scale and location.

Because of the relevance of SPPs for Africa and to account for its diverse climatic settings, a plethora of research exists on the efficiencies and performances of various SPPs, particularly for East Africa (e.g., Ageet et al. 2022; Awange et al. 2016; Diem et al. 2014; Dinku et al. 2008; Geleta and Deressa 2021; Kimani et al. 2017; Romilly and Gebremichael 2011), the central basin region (e.g., Camberlin et al. 2019; Cohen Liechti et al. 2012; McCollum et al. 2000; Serrat-Capdevila et al. 2016), and West Africa (e.g., Dembélé and Zwart 2016; Maranan et al. 2020; Nicholson et al. 2003). Research on the use of various SPPs has considered southern Africa (e.g., De Coning 2013; De Coning and Poolman 2011; Du Plessis and Kibii 2021; Sawunyama and Hughes 2008; Toté et al. 2015). However, to date, little is known about the performance of SPPs in the Western Cape Province of South Africa, a region characterized by a Mediterranean climate with frontal rainfalls as opposed to the mainly convective rain-bearing systems found in the rest of southern Africa (Preston-Whyte and Tyson 1988). An investigation of the performance of different approaches to precipitation estimation from satellite sensors on rainfalls in this Mediterranean climate is therefore necessary.

This paper presents an analysis of several SPPs and reanalysis datasets by considering their performance against observed data from ground-based rainfall gauges in the Western Cape, South Africa, with an aim to evaluate SPP (and reanalysis product) performance in the winter rainfall zone. The analysis was performed over 10 years (2012–21) with a set of station data that largely do not enter the GTS of the World Meteorological Organization. Thus, the unique aspect of this study is that a station ensemble within the Western Cape region is at hand which serves as an independent reference for the analysis of the test datasets. As the need for early warning systems, such as drought and flood monitoring, becomes crucial under a changing climate (e.g., Kreibich et al. 2022; Ward et al. 2020; Yang and Liu 2020; Calvo-Solano and Quesada-Román 2024; Mal et al. 2018), reliable precipitation records are needed, not least since the reduction in precipitation station records since the early 2000s in South Africa requires that SPPs fill data gaps in the historical network. Section 2 describes the study area, and section 3 explains the data and methods used.

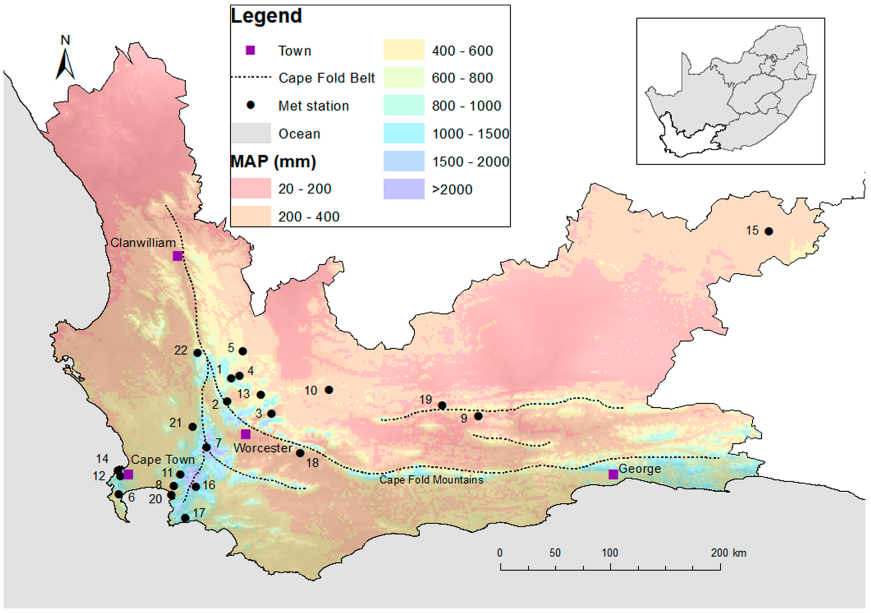

FIG. 1. Mean annual precipitation in the Western Cape Province, South Africa, with the location of the 22 meteorological stations used in this analysis; see Table 1 for cross reference. Data source: Bailey and Pitman (2015).

2. Study area

The Western Cape, South Africa, is the most southwestern province of South Africa (Fig. 1) and is bordered by the Indian Ocean to the south and the Atlantic Ocean to the west (Du Plessis and Schloms 2017). The province has an area of ~129 000 km^2 and a range of climatic and terrain heterogeneity. Topography in the Western Cape is dominated by the Cape Fold Belt Mountains, an L-shaped range of mountains that separate the coast and the dry Karoo interior. The province's climate is characteristically Mediterranean, grading toward arid (Preston-Whyte and Tyson 1988), experiencing summer drought conditions that break when the winter rains of midlatitude cyclonic origin (and associated cold fronts) arrive. Much of the province has a designated Cs Köppen climate (Roberts et al. 2001), while the interior north of the Cape Fold Mountains, however, has a dry desert climate (BW Köppen climate).

Mean annual precipitation ranges between <50 mm along the west coast and interior and >3000 mm in high-elevation regions along the Cape Fold Mountain Belt due to orographic effects (Bailey and Pitman 2015). Rainfall extremes are driven by strong frontal and cutoff low pressure systems (de Waal et al. 2017; Preston-Whyte and Tyson 1988), which can result in cumulative 3-day rainfalls in excess of 300 mm. Analyses of local precipitation samples reveal greater deuterium excesses present in local meteoric water lines (LMWLs) (de Waal et al. 2023; Harris et al. 2010) compared to the global meteoric water line (GMWL) (Craig 1961) suggesting that the primary source of rainfall in the province stems from an arid vapor source (evaporation-derived precipitation)—the cold Southern Ocean (de Waal et al. 2023), in stark contrast to convective rainfalls that occur in other parts of the country, driven by warm, humid air from the east coast of the country (Preston-Whyte and Tyson 1988).

3. Data and methods

The approach of this study was to compare observed rainfall data with precipitation estimates from several widely used SPPs with slightly different rainfall estimation philosophies, namely, CHIRPS (Funk et al. 2015), Integrated Multi-satellitE Retrievals for GPM (IMERG) (Huffman et al. 2017), ERA5 (Hersbach et al. 2020), and MSWEP (Beck et al. 2017). The rationale for the selection of these SPPs was that the various products (such as IMERG and CHIRPS) target different applications (e.g., early warning and drought detection/monitoring). As such, exploring their characteristics and performances is of great importance for planning and decision-making in regions characterized by high interannual rainfall variability. The products selected also represent a range of precipitation estimation methodologies (see Table 2) that weigh PMW sensor inputs or calibration with measured (gauged) data to different extents. To date, there is a limited understanding of which approaches may perform better in Mediterranean climates such as the Western Cape.

To allow for a fair comparison, all SPPs were regridded using the first-order conservative remapping approach ("remapcon") of the Climate Data Operators (CDOs; Schulzweida 2023) to a spatial resolution of 0.25°, which is commonly used for ERA5. Thus, for simplicity, the daily rainfall of all SPPs was interpolated onto the same grid coordinates as ERA5. Conservative remapping is chosen above other methods, such as bilinear interpolation, to ensure the preservation of the domain-averaged rainfall, which becomes important when changing the spatial

TABLE 1. Station metadata for selected rainfall gauges across the Western Cape Province used in the study. Reports from SAWS stations operationally ingested into the GTS are indicated with an asterisk (*).

ID	Station name	Latitude (°)	Longitude (°)	Köppen climate[a]	Elevation (m)	Data record	Observations (*n*)	Source
1	Bokveldskloof	−33.1855	19.3375	Csb	1038	2014–21	2921	ARC
2	Ceres	−33.37	19.307	Csa	457	2012–21	3476	SAWS
3	De Doorns	−33.474	19.665	BSfk	471	2012–21	3408	SAWS
4	Die Erf	−33.166	19.407	Csb	992	2012–21	3453	SAWS
5	Excelsior Ceres*	−32.963	19.43	Csb	958	2012–21	3619	SAWS
6	Fish Hoek	−34.131	18.42	Csb	12	2014–21	2538	SAWS
7	Fizantekraal	−33.7508	19.1346	Csb	744	2012–21	3652	ARC
8	Helderberg Nature Reserve	−34.063	18.869	Csb	141	2012–21	3496	SAWS
9	Hoeko	−33.4896	21.3589	BSfk	614	2012–21	3594	ARC
10	Jan De Boers	−33.275	20.141	BSfk	840	2012–21	3546	SAWS
11	Jonkershoek	−33.967	18.922	Csb	239	2012–19	2906	SAWS
12	Kirstenbosch	−33.986	18.43	Csb	156	2012–21	3638	SAWS
13	Klondyke Farm	−33.315	19.581	Csb	1186	2012–21	3628	SAWS
14	Molteno Reservoir*	−33.937	18.41	Csb	97	2012–21	3645	SAWS
15	Murraysburg	−31.9801	23.7403	BSfk	1193	2012–21	3469	ARC
16	Nuweberg	−34.07	19.047	Csb	572	2012–21	3494	SAWS
17	Oudebosch	−34.323	18.962	Csb	61	2012–21	3411	SAWS
18	Robertson	−33.794	19.901	BSfk	211	2012–21	3630	SAWS
19	Rouxpos	−33.4049	21.0664	BSfk	641	2012–21	3548	ARC
20	Strand	−34.141	18.848	Csb	7	2012–21	3617	SAWS
21	Welbedacht	−33.578	19.019	Csa	190	2012–21	3565	SAWS
22	Zuurvlaakte	−32.9739	19.0614	Csb	1000	2012–21	3652	ARC

[a]Council for Scientific and Industrial Research (2015).

resolutions of SPPs like in this study. The conservative remapping technique in CDO is based on the Yet Another Coupler (YAC) (Hanke et al. 2016) package. More details on conservative remapping can be found in Taylor (2024). With all SPPs being brought to the same grid, a statistical analysis of SPP performance was conducted using a range of univariate and multivariate statistical analysis techniques and categorical validation statistics as described below.

a. Sources of rainfall data

1) GAUGED DATA

Daily rainfall data for 22 rain gauges were obtained from the South African Weather Service's (SAWS) and Agricultural Research Council's (ARC) databases (Table 1). We note that observations of only two stations, i.e., Excelsior Ceres and Molteno Reservoir, are disseminated via the GTS. Thus, since the majority of the stations, to the best of our knowledge, do not enter any calibration procedures within the SPPs used in this study, the station ensemble can generally serve as an independent verification dataset.

Observed data were abstained from 1 January 2012 to 30 December 2021, though most of the rain gauges recorded missing data for part of the data record (Fig. 2). While missing data can affect the performance metrics and validation statistics calculated in this paper, filling gaps in the data would require several problematic assumptions to be made. As such, the authors considered 10 years for data analysis that still gave ~3000 total observations per station (Table 1) to produce robust validation statistics. We did not validate for days where there was missing measured (gauged) data.

Daily data for ARC stations are presented from 0000 to 0000 SAST (2200–2200 UTC), while data from SAWS are recorded from 0800 to 0800 SAST (0600–0600 UTC). Therefore, for comparative purposes, the subdaily SPP (or reanalysis) data were obtained and aggregated to daily (2200–2200 UTC for ARC station comparison and 0600–0600 UTC for SAWS stations) precipitation estimates. These datasets are described below.

2) IMERG V6B AND V7

The IMERG (Huffman et al. 2017), V6B, dataset is a globally gridded precipitation product that integrates data from a variety of sources within the GPM mission constellation satellite network (Tan et al. 2016; Maranan et al. 2020). The GPM

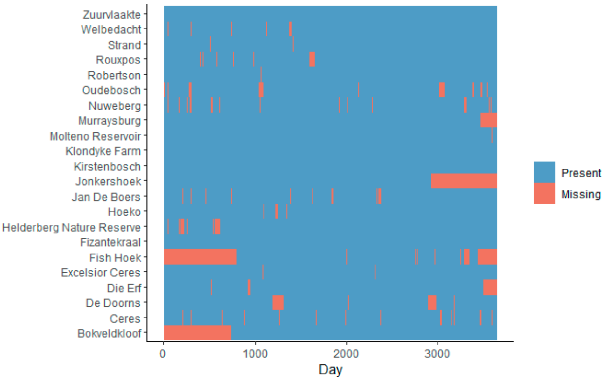

FIG. 2. Length of the daily data record (1 Jan 2012–30 Dec 2021) for each RG with missing data indicated in red.

observation network, centering around the GPM Core Observatory satellite and hosting a dual-frequency precipitation radar (DPR) as well as a 13-channel partner PMW imager (GMI), is augmented by multiple PMW instruments within the GPM constellation and IR information from geostationary satellites (NASA 2023). Rainfall estimates from IMERG are processed on a 0.1° grid at 30-min intervals (Bulovic et al. 2020). Differing in latency and, thus, underlying data availability, IMERG features three runs, two of which—the Early and Final Runs (IMERG-E and IMERG-F, respectively)—are used in this study for the analysis of IMERG version 6B. While IMERG-E is provided after a 6 h delay and with rudimentary spatiotemporal morphing (Tan et al. 2016), IMERG-F is made available after approximately 3 months to accommodate the full morphing procedure as well as the calibration with the ensemble of global gauge data of the considered month. By the time of compiling this study, only the Final Run was processed for the new IMERG, version 7A (IMERG-V7), but it is yet included in the present analysis to provide insights into the performance of an SPP after a version increment. Here, notable changes between V6B and V7 include a bug fix of a spatial offset in gridding precipitation information, an improved intercalibration of PMW estimates, and changes in the morphing scheme by using the Scheme for Histogram Adjustment with Ranked Precipitation Estimates in the Neighborhood (SHARPEN) technique (Tan et al. 2021).

3) CHIRPS v2

The creation of the quasi-global CHIRPS (Funk et al. 2015) dataset, featuring daily, pentadal, and monthly rainfall estimates on a 0.05° grid, contains two major steps. The first step revolves around the determination of the pentadal CHIRPS field, which is a derivative of the averaged field of the global, monthly precipitation dataset CHPclim (Funk et al. 2015—A global satellite-assisted precipitation climatology). Here, pentadal cold cloud duration (CCD) statistics based on thermal IR information are regressed with pentadal rainfall fields of the TRMM Multisatellite Precipitation Analysis (TMPA; Huffman et al. 2010) 3B42 and subsequently used as calibrators of CHPclim, yielding the CHIRP rainfall estimates. Disaggregation to daily estimates is realized based on daily precipitation fields of the Coupled Forecast System (CFS; Funk et al. 2015). In the second step, publicly available daily rainfall station data are incorporated into CHIRP through a modified inverse distance weighting procedure to create CHIRPS. We note that the daily CHIRPS dataset (0000–0000 UTC) does not completely align with the measurement period of the stations (2200–2200 UTC or 0600–0600 UTC). While acknowledging this limitation, we abstained from performing any corrections on daily rainfall values.

4) ERA5

Having been released in 2016, ERA5 (Hersbach et al. 2020) is the fifth major global reanalysis produced by the European Centre for Medium-Range Weather Forecasts (ECMWF) and is based on a 4DVar data assimilation scheme within the model cycle 41r2 of the Integrated Forecasting System (IFS). ERA5 fields are available on an hourly basis at a spatial resolution of 31 km as well as on 91 vertical model levels for four-dimensional parameters. For this study, ERA5 "total precipitation" was obtained from the Copernicus Data and Services (CDS; Copernicus 2023) on an hourly basis at a 0.25° × 0.25° latitude–longitude grid. It was then temporally aggregated according to the measuring periods of the rain gauges indicated in section 3a(1) at the nearest grid points. It shall be noted that precipitation observations, e.g., from rain gauges and radars, are not assimilated outside of the United States (Lavers et al. 2022). Only over the sea, rain-affected microwave radiances are assimilated. Therefore, ERA5 precipitation is primarily a model-driven short-term forecast field over the study domain.

5) MSWEP V2.8

The MSWEP, V2.8, is a global precipitation dataset and is available for the period 1979–2020 (historical MSWEP) at 3-hourly intervals with a 0.1° spatial resolution (Beck et al. 2017, 2019). MSWEP precipitation estimates are created through an optimally weighted averaging technique using 1) remotely sensed PMW-based satellite data (IMERG-Late), 2) reanalysis data (ERA5), and 3) rain gauge observations [Global Surface Summary of the Day (GSOD), Global Historical Climatology Network–Daily (GHCN-D), several national databases] (see technical documentation on MSWEP, V2.8; https://www.gloh2o.org/mswep/). The product was designed primarily for hydrological modeling applications (Lakew et al. 2020; Sun et al. 2022) and combines the data such that weights are assigned at every location depending on the quality and availability of the underlying data sources. The temporal resolution of MSWEP does not allow a complete temporal overlap with the measuring periods of the reference gauges in this study. Therefore, MSWEP was aggregated within the closest possible times, i.e., 2100–2100 UTC for the ARC stations and 0900–0900 UTC for the SAWS stations. A summary of the selected SPPs is presented in Table 2.

b. SPP efficiency evaluation

The daily SPP (or reanalysis data) value for each grid point (termed "pixel") was compared to the observed data of the gauge located within that pixel. Categorical validation statistics were calculated for each SPP at each station. These statistics are derived from a cross tabulation, where hits H, false alarms F, misses C, and correct negatives N were calculated based on a contingency table (Table 3) (cf. Ageet et al. 2022). The threshold to distinguish dry and wet days is set to 0.2 mm day^{-1}.

The categorical validation statistics (Table 4) calculated are 1) the probability of detection (POD) which describes the fraction of correctly predicted events, 2) the probability of false alarm (POFA) which calculates the fraction of forecasted events that did not occur, 3) the bias in detection (BID) score, and 4) the Heidke skill score (HSS) which measures the accuracy of the estimates accounting for matches due to random chance. Correlation, root-mean-square error (RMSE), and variance statistics for each SPP at each station were calculated. These statistics were then presented on a Taylor diagram (Taylor 2001). The

TABLE 2. Details on the selected SPP products regarding major input data and the native spatial and temporal resolutions.

SPP	Major data input	Native spatial resolution	Temporal resolution	Reference
CHIRPS v2	IR, RGs	0.05°, 0.25°	Daily (0000–0000 UTC)	Funk et al. (2015)
ERA5	Reanalysis (IFS, Cy41r2)	0.28125°	Hourly	Hersbach et al. (2020)
IMERG (V06B Early/Final and V07A Final)	PMW, IR, RGs	0.1°	Half-hourly	Huffman et al. (2017)
MSWEP (V2.8)	PMW, RGs, reanalysis	0.1°	3-hourly (starting at 0000 UTC)	Beck et al. (2017, 2019)

Taylor diagram presents the Pearson correlation, centered RMSE (CRMSE), i.e., the RMSE minus the bias, and a comparison of the standard deviations between two datasets (observed and simulated rainfall) with a single point on a 2D graph (Taylor 2001). We note that the standard deviation and the CRMSE are normalized to enable a region-independent comparison of the stations and the nearest product pixels. As an extension to the classical Taylor diagram, the bias is included and is represented by arrows originating at the data points (cf. Fig. 9 in Ageet et al. 2022). Here, the bias shares the same (radial) axis, and therefore, unit and magnitude are the same as for CRMSE and indicate positive (negative) values if the arrow points away from (toward) the observation point (red square). Mean absolute error (MAE), percent bias (PB), and Nash–Sutcliffe efficiencies (NSEs) were also calculated (Table 4).

c. SPP performance in the estimation of extreme events

The ability of satellite-based sensors to estimate extreme precipitation events is of great importance, particularly for hydrometeorological monitoring and management. For instance, large streamflows are often driven by daily rainfall extremes (de Waal et al. 2017) that characterize hydrometeorological hazards. These extreme events are not only linked to flooding but are also of great importance in that they refill reservoirs (Holloway et al. 2012). For this analysis, an extreme event is defined as a daily rainfall that exceeds the 95th percentile of rain days (the latter defined as a day with ≥0.2 mm) in the observed (gauged) data. The 95th percentile threshold values were calculated for individual stations, and the corresponding daily SPP estimates for those days were obtained.

4. Results

The results of this SPP analysis consider the performance of the six SPPs through a variety of metrics including categorical validation statistics and descriptive statistics of bivariate data. First, a station-by-station performance of the SPPs for annual and daily rainfalls and overall SPP performance across all stations is reported and visualized spatially. Second, the ability of the selected SPPs to predict rainfall extremes is considered. Third, spatial differences in SPP performances are described. Finally, the impact of spatial grid (pixel) resolution on our validation statistics is discussed.

TABLE 3. Contingency table for calculating satellite precipitation product hits H, misses m, false alarms F, and correct negatives N.

	Observed ≥ 0.2 mm	Observed < 0.2 mm
SPP ≥ 0.2 mm	Hit H	False alarm F
SPP < 0.2 mm	Miss M	Correct negative N

a. SPP performance for mean and intense rainfalls

Daily observed rainfall data were accumulated annually and compared with the aggregate SPP predicted rainfall for each gauge. All SPPs tended to underestimate rainfall at an annual scale, although this is not necessarily true for each individual station, e.g., De Doorns, Jan de Boers, Robertson, and Strand (Table 5). In particular, the IMERG-E underestimated rainfall by the largest amount (0.64). The best-performing products in this regard were ERA5 (0.91) followed by the CHIRPS product (0.86). Certain stations (Ceres, Jonkershoek, Kirstenbosch, Nuweberg, Oudebosch, and Zuurvlakte) showed consistently poor SPP performance for all products. Die Erf, Fish Hoek, Murraysberg, Robertson, Rouxpos, and Strand displayed stronger model performance, i.e., within a 5% difference, when aggregated to annual data.

The spatial distribution of these results for ERA5—selected for representation as the best-performing SPP (Tables 6 and 7)—(Fig. 3) suggests that no spatial pattern to the results exists. Notably, the worst-performing stations (2, 11, 12, 16, 17, and 22) are located in mountainous regions associated with the Cape Fold Belt. However, several stations in these mountainous regions perform well (e.g., 7, 21).

When considering the mean categorical validation statistics for daily data (across all observation stations) (Table 6, Fig. 4), the ERA5 product again performed the best in a variety of metrics including POD, HSS, r, MAE, RMSE, and NSE, closely followed by MSWEP, which also performs well. Regarding POD, the reanalysis-driven products ERA5 and MSWEP (both at 0.85) considerably outperform all other SPPs. Additional analysis shows that both datasets exhibit the highest wet-day frequency of all (Table A3, in the appendix), which explains the higher detection ability of rainfall as well as the highest BID values among all SPPs to some extent. However, ERA5 and MSWEP also belong to the products with the lowest POFA, suggesting that the performance regarding the assignment of rainfall on a daily time scale is enhanced when reanalysis data are involved. Overall, this is reflected in the highest (lowest) values for HSS, r, and NSE (MAE and RMSE). CHIRPS behaves the opposite and appears to struggle with a dichotomous wet-/dry-day distinction over the Western Cape

TABLE 4. Summary of validation statistics used in the analysis where H, F, M, and N represent hits, false alarms, misses, and correct negatives, respectively, and x_i and y_i represent observed rainfalls (at gauge) and SPP estimates, while x and y represent the means of gauged observations and SPP estimates, respectively. Statistic ranges and optimal scores are also presented by Ageet et al. (2022). The bold font indicates the optimal value.

Statistic	Range and optimal value	Formula	Description
POD	[0, 1] **1**	$\frac{H}{H+M}$	Satellite's ability to correctly detect rainy days
POFA	[0, 1] **0**	$\frac{F}{H+F}$	Proportion of SPP-predicted rain events that were not observed
BID	[−∞, +∞] **1**	$\frac{H+F}{H+M}$	Assessment of whether SPP overestimates or underestimates rainy day frequency
HSS	[−∞, 1] **1**	$\frac{2(HN-FM)}{(H+M)(M+N)+(H+F)(F+N)}$	Assesses the skill of SPPs compared to random chance
r	[−1, 1] **1**	$\frac{\sum_i^n (x_i-\bar{x})\sum_i^n (y_i-\bar{y})}{\sqrt{\sum_i^n (x_i-\bar{x})}\sqrt{\sum_i^n (y_i-\bar{y})}}$	Assesses covariance of the gauged data with that of the SPP
MAE	[0, +∞] **0**	$\frac{1}{n}\sum_i^n \lvert(y_i-x_i)\rvert$	Measures bias of the SPP regardless of direction
PB	[−∞, +∞] **0**	$100\times\frac{\frac{1}{n}\sum_i^n (y_i-x_i)}{\bar{x}}$	Assesses tendency of SPP to underestimate or overestimate rain rates relative to the mean of the observed data
RMSE	[0, +∞] **0**	$\sqrt{\frac{1}{n}\sum_i^n (y_i-x_i)^2}$	Measures the bias of the SPP but assigns more weight to outliers
NSE	[−∞, 1] **1**	$1-\frac{\sum_i^n (x_i-y_i)^2}{\sum_i^n (x_i-\bar{x})^2}$	NSE describes the predictive accuracy of models relative to the observed data

region. Its correlation coefficient value, the lowest among all products (0.25), also shows that estimating daily rainfall patterns imposes a major challenge for CHIRPS, as opposed to its reasonable estimation of annual rainfall totals. With respect to the IMERG products, both the monthly rainfall calibration (IMERG-E vs IMERG-F) and a version change (IMERG-F vs IMERG-V7) have led to a performance improvement in almost every aspect. However, this does not include the performance around daily extremes (i.e., >95th percentile), where, in fact, all SPPs struggle. NSE is negative for all products, indicating that their "predictive" skill of daily extreme values is inferior to the mean observed value of this sample.

Concerning SPP performance in predicting extreme rainfalls, the ERA5 product again came out tops with the best MAE, RMSE, and NSE and the second-best r. All SPPs exhibit poor performance in relation to extremes, and none of the products appear to have a good relationship in the algorithm between input information and rainfall rate. Strong underestimation of extreme values is evident, where, however, CHIRPS performs best. All NSE values are negative for extremes, meaning that the mean of the observations/gauges is greater than those of the SPPs.

SPP performance differs by season (Fig. 5). Notably, POD for all SPPs is highest during the rainy season (austral winter) of June–August (JJA), while the POFA is lowest in this season as well. ERA5 and MSWEP consistently show the greatest BID across all seasons, though this is most pronounced in austral summer (DJF) (Fig. 5c). For all SPPs, the HSS was highest in JJA and lowest in austral summer. Thus, it can be argued that the performance of all SPPs is enhanced as soon as rainfall originates from synoptic-scale atmospheric patterns, most prevalent in austral winter. Regarding the individual performances of the SPPs, seasons largely do not affect the performance ranking of the products evaluated in Table 5.

A compacted view of the performance of each SPP is presented in the Taylor diagram (Fig. 6). First of all, all SPPs generally underestimate the observed variability of daily rainfall, as indicated by the position of the data points well within the red solid quarter circle (i.e., observed standard deviation of daily rainfall). Here, the rainfall variability is underestimated the most by the reanalysis-driven products ERA5 and MSWEP as well as IMERG-E and is least underestimated by CHIRPS. Since the magnitude of the standard deviation is strongly controlled by high values in the case of precipitation, this finding is closely related to the ability of the SPPs to

TABLE 5. The proportion of observed annual rainfall at a 0.25° common grid (optimal value = 1).

ID	Station	CHIRPS	ERA5	IMERG_E	IMERG_F	IMERGV7	MSWEP	SPP mean
1	Bokveldkloof	0.63	0.82	0.42	0.61	0.44	0.66	0.60
2	Ceres	0.48	0.56	0.27	0.41	0.37	0.45	0.42
3	De Doorns	1.23	1.40	0.91	1.22	1.04	1.24	1.17
4	Die Erf	1.14	1.28	0.77	1.11	0.88	1.10	1.05
5	Excelsior (Ceres)	0.84	1.00	0.69	0.86	0.71	0.86	0.83
6	Fishhoek	0.89	1.10	0.74	0.90	1.05	1.00	0.95
7	Fizantekraal	1.21	1.16	0.52	0.81	0.81	1.03	0.93
8	Helderberg Nature Reserve	0.94	1.00	0.51	0.82	0.84	0.86	0.83
9	Hoeko	0.98	0.80	0.86	0.83	0.87	0.81	0.86
10	Jan De Boers	1.07	1.11	1.28	1.37	1.22	1.07	1.18
11	Jonkershoek	0.56	0.68	0.30	0.51	0.54	0.68	0.55
12	Kirstenbosch	NA	0.43	0.29	0.47	0.50	0.39	0.42
13	Klondyke	0.72	0.87	0.53	0.75	0.60	0.74	0.70
14	Molteno	NA	0.86	0.58	0.94	1.01	0.79	0.84
15	Murraysberg	0.59	0.91	1.59	0.89	0.89	0.86	0.96
16	Nuweberg	0.58	0.60	0.28	0.46	0.48	0.59	0.50
17	Oudebosch	0.52	0.56	0.34	0.52	0.57	0.58	0.52
18	Robertson	1.12	1.19	0.76	1.04	1.05	1.10	1.04
19	Rouxpos	1.18	0.93	1.06	1.07	1.12	0.95	1.05
20	Strand	1.11	1.01	0.70	1.03	1.13	1.01	1.00
21	Welbedacht	1.12	1.16	0.46	0.74	0.74	0.95	0.86
22	Zuurvlakte	0.37	0.51	0.22	0.32	0.29	0.39	0.35
	Mean	0.86	0.91	0.64	0.80	0.78	0.82	0.80

resolve extreme values, which will be addressed again later. In contrast, ERA5 and MSWEP (CHIRPS) show the highest (lowest) correlation coefficient among the SPPs. As mentioned earlier, this suggests that the reanalysis-driven products are best at reproducing daily rainfall patterns, an aspect that CHIRPS fails to do. Furthermore, ERA5 and MSWEP are closest to the minimum normalized CRMSE (dashed red semicircle), meaning that they can keep random errors low at their respective correlation coefficient value. Compared to the other SPPs, neither of the Final Runs of IMERG particularly excels in any of the aspects just mentioned but, overall, obtains the highest Taylor score, mainly by exhibiting the closest match to the standard deviation of the stations. All SPPs show a negative bias in rainfall estimation (arrows directed toward the reference point) with the IMERG-E product showing the greatest bias (magnitude of the arrow).

Delving deeper into the representation of daily rainfall, Fig. 7 illustrates quantile–quantile (QQ) plots based on the entire sample of wet days in the rain gauges and SPP, respectively (Fig. 7a), and based on the subset of hits (Fig. 7b), i.e., instances where both rain gauge and SPP exhibit rainfall. Regarding the entire sample, the curves of all SPPs are located under the diagonal, expressing an underestimation of daily rainfall values at virtually all quantiles (Fig. 7a). This can be attributed to two main reasons. First, The SPPs overestimate the occurrence of low-intensity rainfall, leading to a deviation

TABLE 6. Validation statistics and performance metrics for the SPPs evaluated in the study at a common grid of 0.25°. The value of the best-performing SPP in a category is indicated in bold. The contingency-related metrics POD, POFA, BID, and HSS are not performed for daily extremes. The sample of daily extremes consists of all RG-based daily rainfall greater than the 95th percentile value of the wet-day sample.

Time step	SPP	POD	POFA	BID	HSS	*r*	MAE	PB	RMSE	NSE
Daily	CHIRPS	0.47	0.56	1.07	0.32	0.25	8.58	−0.77	16.48	−0.22
	ERA5	**0.85**	0.49	1.68	**0.52**	**0.57**	**6.10**	−0.84	**12.69**	**0.26**
	IMERG-E	0.54	0.54	**1.16**	0.36	0.31	8.22	**−0.17**	15.61	−0.12
	IMERG-F	0.59	0.51	1.20	0.41	0.47	7.45	−0.35	14.09	0.08
	IMERG-V7	0.61	**0.47**	**1.16**	0.45	0.49	7.22	−0.36	13.85	0.12
	MSWEP	**0.85**	0.50	1.70	**0.51**	**0.56**	6.19	−0.68	12.87	0.23
Daily extremes (95th percentile)	CHIRPS	—	—	—	—	0.08	42.27	0.72	53.08	−1.91
	ERA5	—	—	—	—	0.16	**32.51**	0.56	**44.06**	**−1.19**
	IMERG-E	—	—	—	—	0.01	39.93	0.68	50.35	−1.86
	IMERG-F	—	—	—	—	0.10	32.50	**0.47**	44.29	−1.24
	IMERG-V7	—	—	—	—	0.11	33.22	0.50	45.10	−1.30
	MSWEP	—	—	—	—	**0.17**	33.78	0.59	45.18	−1.24

TABLE 7. HSS by station for all SPPs at a 0.25° resolution.

ID	Station	CHIRPS HSS	ERA5 HSS	IMERG-E HSS	IMERG-F HSS	IMERG-V7 HSS	MSWEP HSS
1	Bokveldkloof	0.39	0.57	0.41	0.45	0.43	0.56
2	Ceres	0.30	0.54	0.37	0.42	0.44	0.55
3	De Doorns	0.25	0.28	0.33	0.37	0.37	0.29
4	Die Erf	0.26	0.40	0.33	0.39	0.40	0.42
5	Excelsior (Ceres)	0.36	0.61	0.41	0.47	0.45	0.63
6	Fishhoek	0.32	0.57	0.41	0.39	0.50	0.56
7	Fizantekraal	0.31	0.34	0.28	0.32	0.36	0.37
8	Helderberg Nature Reserve	0.34	0.56	0.36	0.38	0.46	0.53
9	Hoeko	0.29	0.46	0.34	0.40	0.45	0.47
10	Jan De Boers	0.15	0.23	0.20	0.23	0.24	0.24
11	Jonkershoek	0.35	0.58	0.33	0.37	0.40	0.54
12	Kirstenbosch	NA	0.65	0.35	0.38	0.52	0.59
13	Klondyke	0.35	0.60	0.36	0.42	0.42	0.62
14	Molteno Reservoir	NA	0.71	0.39	0.40	0.58	0.65
15	Murraysberg	0.33	0.38	0.42	0.48	0.48	0.42
16	Nuweberg	0.36	0.50	0.33	0.39	0.41	0.46
17	Oudebosch	0.34	0.47	0.41	0.42	0.44	0.47
18	Robertson	0.30	0.52	0.29	0.35	0.39	0.52
19	Rouxpos	0.28	0.34	0.32	0.36	0.46	0.37
20	Strand	0.37	0.60	0.46	0.51	0.54	0.61
21	Welbedacht	0.33	0.55	0.35	0.41	0.46	0.53
22	Zuurvlakte	0.33	0.59	0.29	0.33	0.32	0.55

of the SPP curves from the 1:1 line to the negative side already at lower percentiles. Second, the SPPs are unable to resolve the extremes. The latter is particularly prevalent for the reanalysis-driven products ERA5 and MSWEP, whose maximum values underestimate those of the observations by more than 200 mm. The inability of these two products to capture the extremes is reflected by the strongest underestimation of the rainfall variability (i.e., normalized standard deviation) compared to that of the observation in the Taylor diagram in Fig. 6. Furthermore, the rainfall distribution of the SPPs underpins the underestimation of rainfall totals on an annual time scale (see Table 5).

Among all SPPs, CHIRPS is the least prone to this overestimation tendency of low-intensity rainfall. Furthermore, CHIRPS shows the highest potential in resolving extreme daily rainfall, based on the maximum value in Fig. 7, but

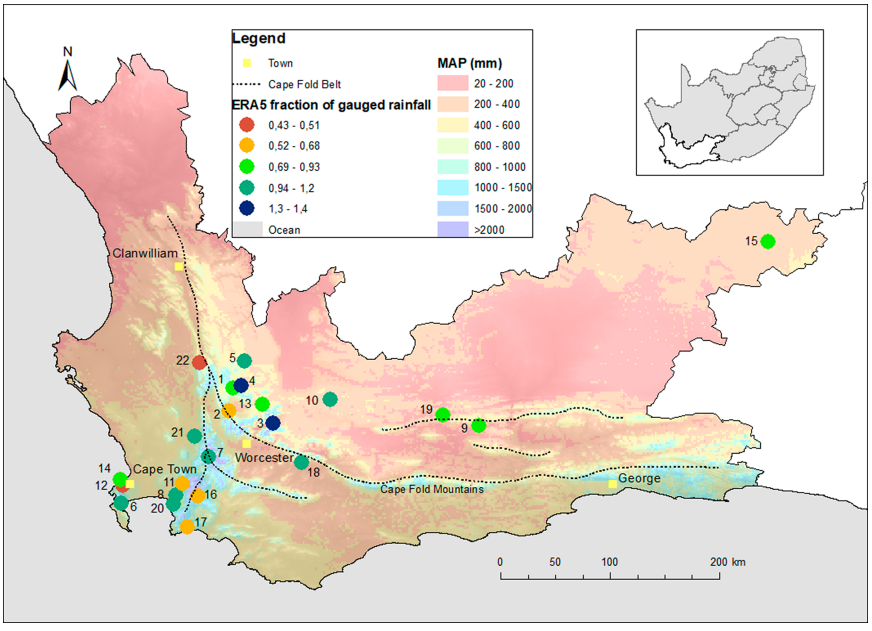

FIG. 3. ERA5 prediction of annual rainfall at 0.25° resolution compared to observed data at each rainfall gauge.

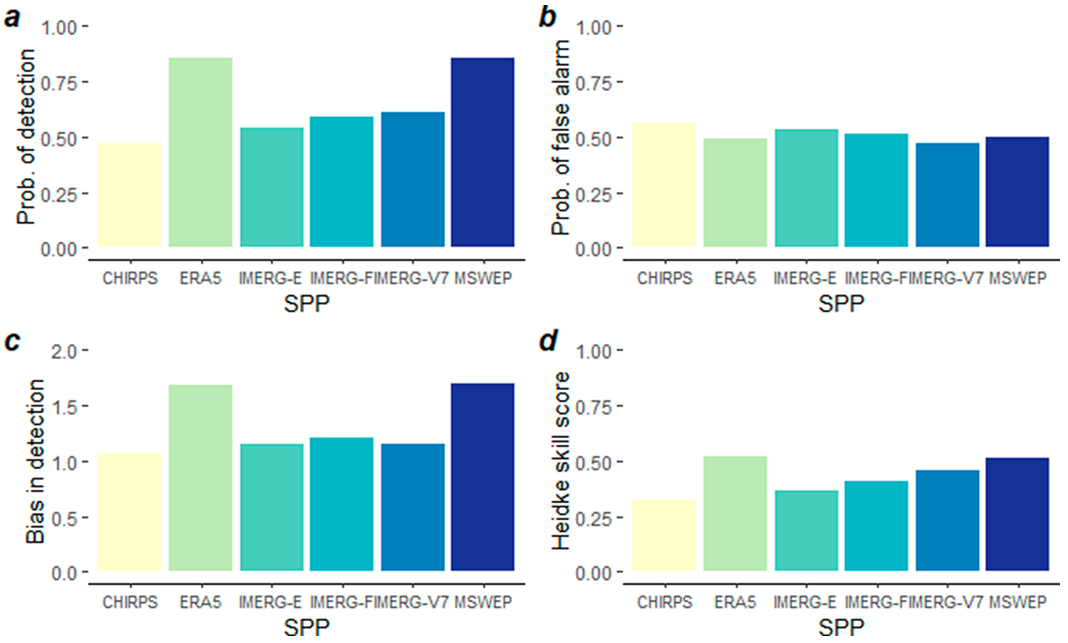

FIG. 4. Visual representation of mean SPP/reanalysis product (collectively termed SPP) performance (0.25° resolution) for all observation stations based on categorical validation statistics for (a) POD, (b) POFA, (c) BID, and (d) HSS.

more so if its native resolution (0.05°) is considered (not shown). Regarding the sample of hits only (Fig. 7b), i.e., excluding misses and false alarms, an improved representation of the lower quantiles of daily rainfall by ERA5 and MSWEP is evident, whereas all other SPPs exhibit the same features as for the entire sample of wet days (Fig. 7a). Thus, together with CHIRPS, the reanalysis-driven SPPs appear to have a superior treatment of weak to moderate rainfall when they

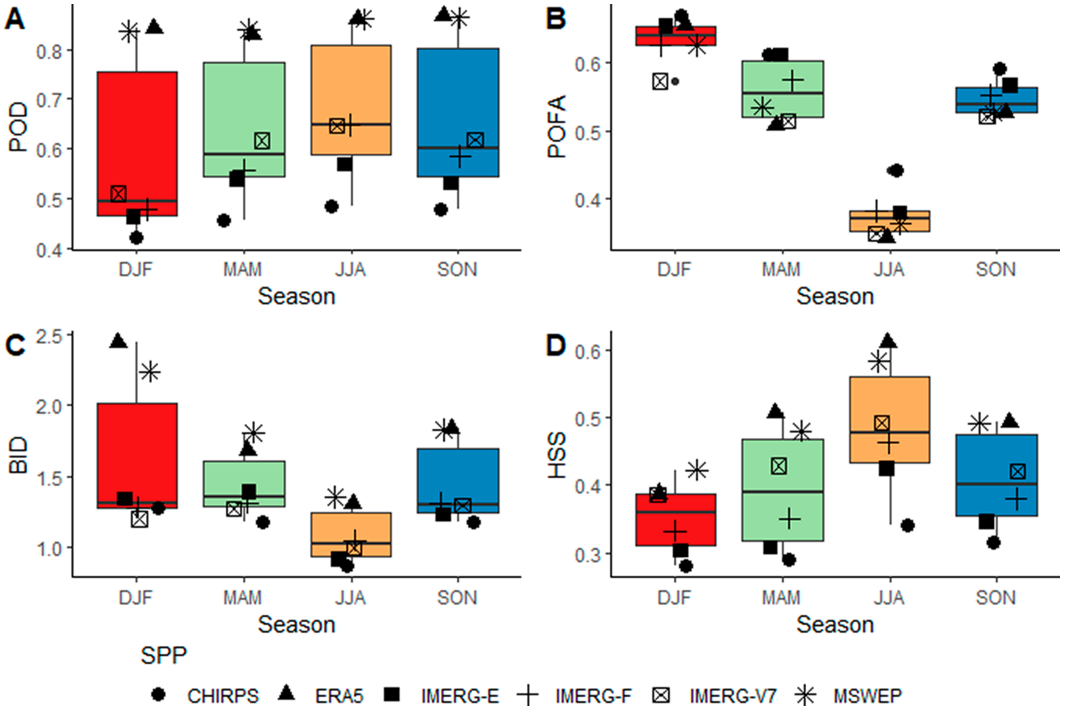

FIG. 5. Mean seasonal validation statistics for each SPP at 0.25° resolution considered in the study: (a) POD, (b) POFA, (c) BID, and (d) HSS.

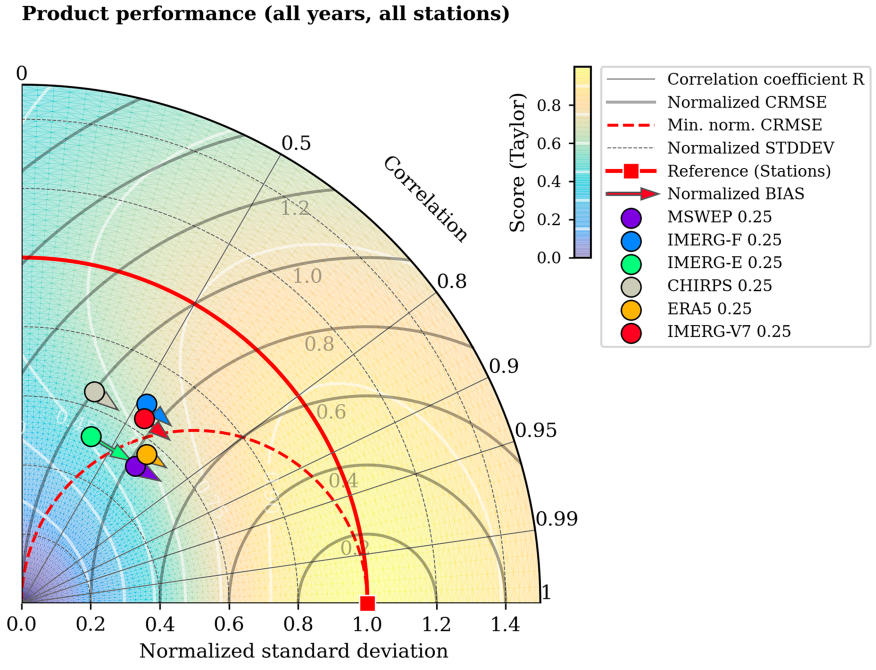

FIG. 6. Taylor diagram for all SPPs considered at a spatial resolution of 0.25°, aggregated from all stations and across the entire data record. Note that the bias is represented as arrows originating from the data points, where they indicate a negative (positive) bias if they point toward (away from) the reference point (red square). The values of the bias, which is aligned to the axis of CRMSE, are defined by the length of the arrows. The Taylor score as defined in Taylor (2001) is indicated by the color-shaded background and white isolines.

are observed in both products. However, strong underestimation tendencies at extreme quantiles remain.

A closer look into the perceptivity and handling of extreme rainfall (i.e., >95th percentile) is given in Fig. 8. Here, the rainfall distribution within the SPPs is compared with that of the rain gauges when extreme rainfall is registered by the latter (Fig. 8a) and vice versa (Fig. 8b). On the one hand, when extreme rainfall events occur, all SPPs struggle severely with

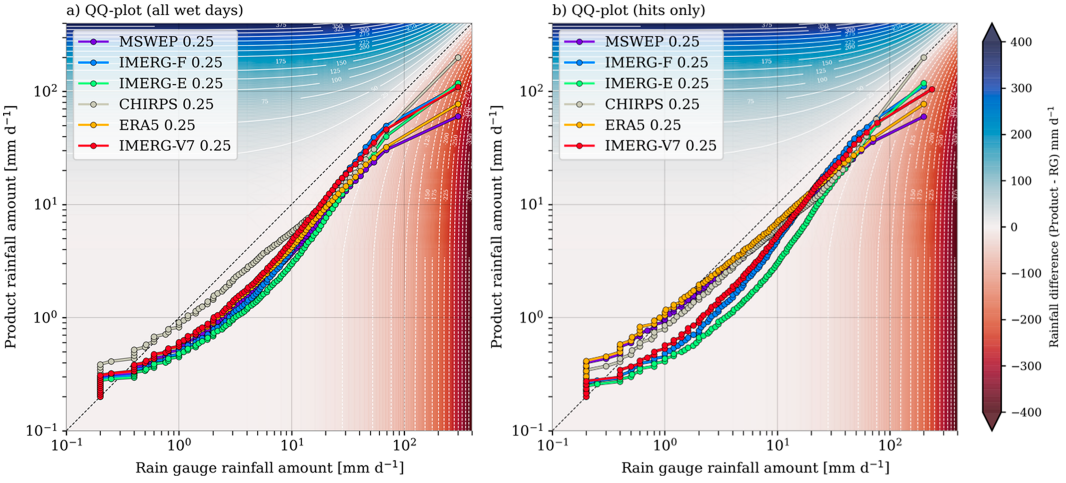

FIG. 7. QQ plots showing the quantile values of daily rainfall, aggregated over all stations (x axis) and nearest pixels (y axis), for the entire study period for two samples: (a) all rainy days (>0.2 mm day^{-1}) and (b) all instances of hits where both RGs and the respective product are rainy. The dashed black diagonal represents the 1:1 line, indicating equal quantile values between observation and SPP if they fall on it. Note that the axes are scaled logarithmically. The colored shading and white isolines denote the differences between quantile values in millimeters per day with red (blue) shading indicating an underestimation (overestimation) by the SPP.

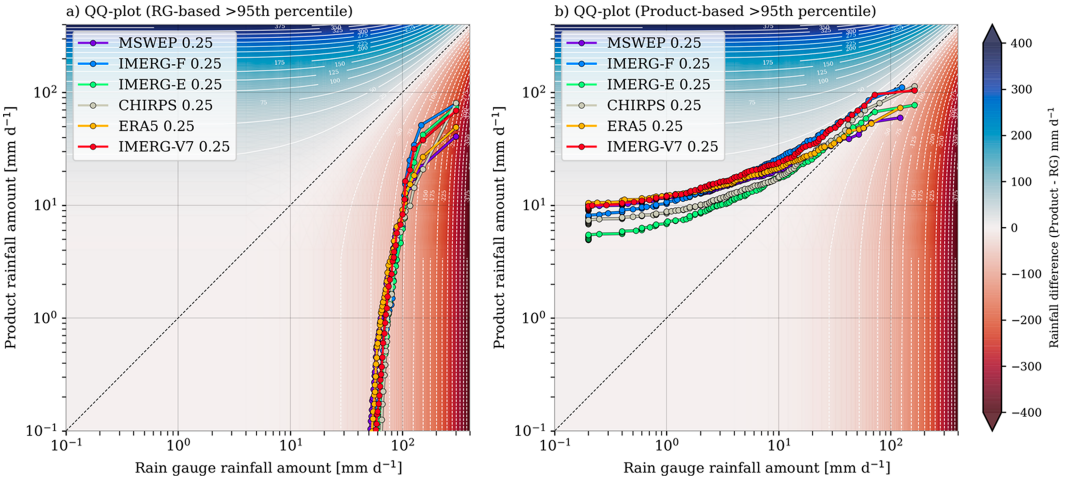

FIG. 8. As in Fig. 6, but for extreme rainfall (i.e., rainfall > 95th percentile) as seen by (a) the RGs and (b) the SPPs. In (a), the sample of the SPPs is created by taking the rainfall values on the same days where extreme rainfall is registered by the RGs, vice versa for (b).

capturing them as seen by the strong negative deviation of all curves from the 1:1 line (Fig. 8a). On the other hand, when SPPs detect extreme rainfall, it does not necessarily align with observation (Fig. 8b), as seen by the distinct positive deviation of the curves from the 1:1 line at most quantiles. These findings resonate with the negative NSE values regarding daily extremes for all SPPs in Table 6, suggesting that the error variance in rainfall magnitude is smaller if simply the observed mean value is taken. Overall, "misses" and "false alarms" of extreme daily rainfall are a prevalent deficiency across all SPPs, leading to low correlations and large errors as seen in Table 6. This behavior is not exclusive to the Western Cape region but also to other parts of Africa (e.g., Monsieurs et al. 2018; Ageet et al. 2022).

b. *Spatial differences in SPP performance*

Spatially, SPP performance is heterogeneously distributed. Consider that for the ERA5 product (Fig. 9), the HSS is higher for many stations in the southwestern region of the Western Cape but falls toward the interior and east of the province. The highest HSSs are found at the Kirstenbosch (12) and Molteno Reservoir (14) rain gauges. HSS is lower at De Doorns (3), Hoeko (9), Jan de Boers (10), and Rouxpos (19) further inland with a notable outlier to this spatial

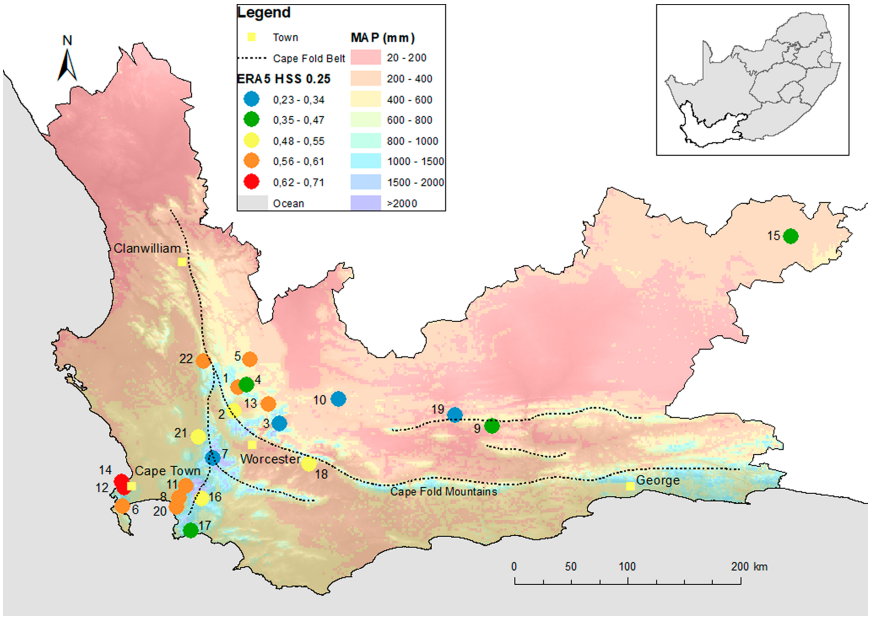

FIG. 9. HSS for ERA5 at each rainfall gauge at 0.25° spatial resolution.

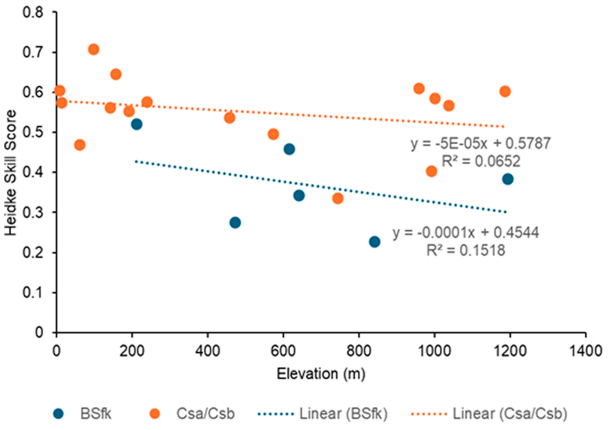

FIG. 10. ERA5 0.25° resolution HSS by elevation and climate zone.

pattern at Fizantekraal (7) in the Boland Mountains. Molteno Reservoir (14) also had the highest HSS for the IMERG-V7 and MSWEP products (Table 6).

A similar spatial pattern for HSS for most SPPs exists. It is noteworthy that the ERA5 and MSWEP products show remarkable similarity in performance at each gauge with the top-performing gauges for each SPP being similar. This insinuates that ERA5 enters MSWEP with the highest weight over the Western Cape region. CHIRPS lags in overall performance when compared to the other SPPs at daily temporal and 0.25° spatial resolutions. The IMERG-V7 product sees improved performance from the Early and Final versions, with the most noticeable jump taking place at Molteno Reservoir (14), a synoptic station.

How station elevation or climatic zones might influence the HSS for each site is addressed in Fig. 10. Based on a *t* test, the HSSs for BSfk climate zone stations are significantly ($p \leq 0.05$) lower than the HSSs for rainfall gauges falling in either Csa or Csb classes. There is little correlation between station elevation and HSS for the ERA5 product (see regression equations in Fig. 10).

c. *Point-to-pixel aspects*

The analyses in previous sections are based on a simple point-to-pixel comparison. However, deficiencies of this approach are commonly known since spatially averaged rainfall in the form of pixel information is analyzed against point measurements from stations, with the latter being unable to account for the within-pixel rainfall variability if considered in an isolated fashion. Thus, this section examines changes in the performance of the products when aggregated information from more than one station within a given pixel is considered as a reference.

For the Taylor diagram in Fig. 11, all SPPs were coarse-grained to a spatial resolution of 0.5° to obtain a pixel that

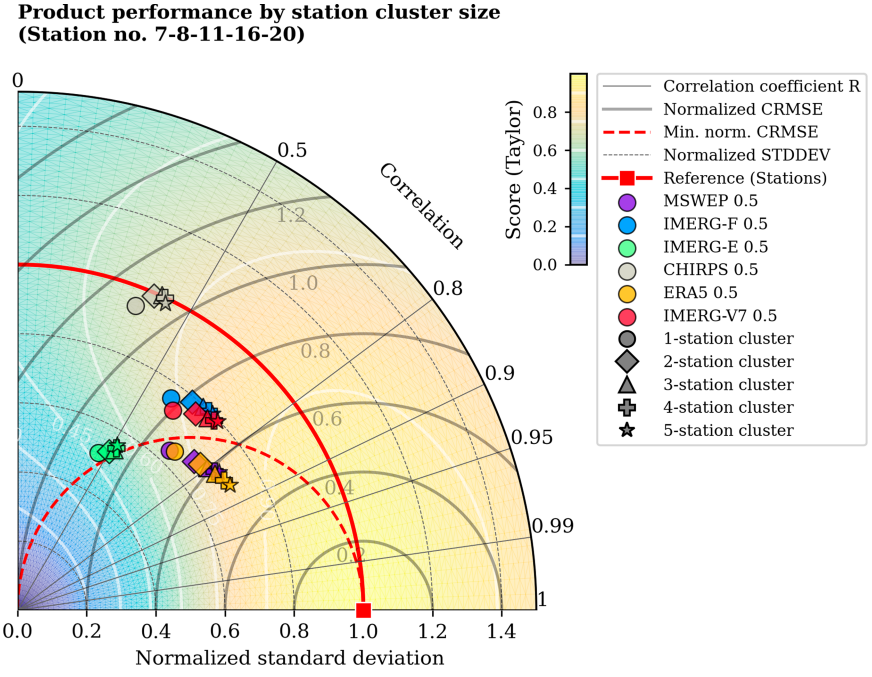

FIG. 11. Taylor diagram showing the performance of the products as a function of the number of aggregated stations as the "point" reference. Here, four stations [viz., Helderberg Nature Reserve (8), Jonkershoek (11), Nuweberg (16), Strand (20)] are within the grid point at (34°S, 19°E) of the coarse-grained products at $dx = 0.5°$ resolution. Daily rainfall data of multistation clusters (i.e., $n = [2, 4]$) are arithmetically averaged values based on all stations involved. The data points represent the averaged metrics and scores from all station combinations (e.g., for the 3-station cluster, possible combinations are 8–11–16, 8–11–20, 8–16–20, etc.).

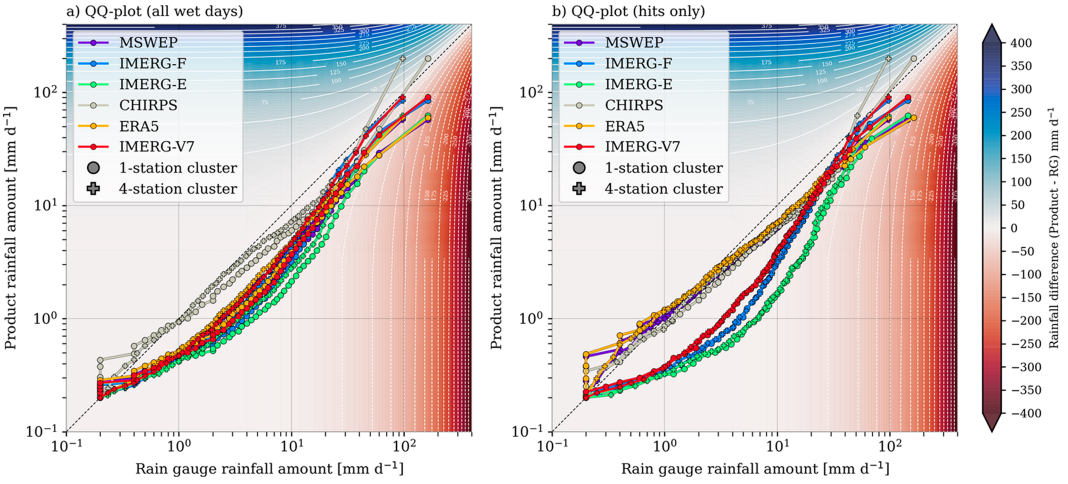

FIG. 12. As in Fig. 7, but based on 1-station (curves with circle markers) and 4-station clusters (curves with plus sign markers) within a coarse-grained 0.5° grid point at (34°S, 19°E), consisting of the stations Helderberg Nature Reserve (8), Jonkershoek (11), Nuweberg (16), Strand (20). Daily rainfall data of the 4-station cluster are arithmetically averaged values based on all stations involved.

includes four stations, namely, (8) Helderberg Nature Reserve, (11) Jonkershoek, (16) Nuweberg, and (20) Strand. We note that the data represent averaged scores based on all possible station combinations. Overall, the more stations are taken into account, the better the SPPs perform, particularly concerning the correlation coefficient, which overall decreases CRMSE. This becomes evident especially for the Final Runs of IMERG as well as the reanalysis-driven products ERA5 and MSWEP. Otherwise, the SPPs remain in the same performance groups within the Taylor diagram as in the results shown earlier. Therefore, it can be concluded that coarse-graining cannot entirely mask major deficiencies of the SPPs by any means. It remains to be seen whether the implementation of more stations within the pixels of the SPPs at their native resolutions yields similar results or even larger performance jumps.

An impression of how the inclusion of more than one station within a pixel influences the rainfall distribution is given in Fig. 12, like Fig. 7, for both all wet days (Fig. 12a) and hits only (Fig. 12b). Here, a comparison is depicted between 1-station (circles) and 4-station clusters (crosses). In principle, station-based daily rainfall amounts experience a decrease with 4-station clusters at almost all percentiles, generally leading to a shift of the curves to the left (Fig. 12a). Consequently, the aforementioned underestimation of daily rainfall is attenuated for all products, most evidently for the highest percentiles. Thus, the largely severe underestimation of extreme rainfall is mitigated accordingly (Figs. 12a,b). For CHIRPS in particular, the latter even results in an overcompensation toward a stronger overestimation which, however, is likely pixel specific. Overall, this exercise substantiates the often-ignored fallacy of the point-to-pixel comparison approach due to the inability of SPPs to resolve subgrid-scale variability of rainfall, particularly at the extreme end. The inclusion of more than one station, if at hand, improves the spatial representation of rainfall within a pixel as well as the assessment of SPP performances.

5. Summary and conclusions

This study provides a detailed synopsis of the performance of six SPPs and reanalysis-driven datasets, namely, CHIRPS, ERA5, MSWEP, and IMERG (Early and Final Runs of V6B, Final Run of V7) in the Western Cape region. It is motivated by the necessity of suitable gridded precipitation datasets to complement a gradually degrading station network in South Africa, and in perspective to secure the means to perform reliable early warning services against (hydro)meteorological hazards for the understudied Mediterranean climate in Western Cape region. Daily rainfall data from 22 stations of SAWS and ARC were applied as a reference against which the test rainfall products, all remapped on a common 0.25° spatial grid, were compared. These SPPs were evaluated on a daily time scale using various error and skill metrics. Finally, they were coarse grained to a spatial resolution of 0.5° to investigate their performance as a function of the number of embedded stations within a single grid cell. The following results stand out:

- On a daily time scale, the reanalysis-based products ERA5 and MSWEP generally outperform all other SPPs with respect to a dichotomous wet-/dry-day distinction and temporal rainfall pattern, exhibiting the highest HSS and correlation coefficient, respectively. The strongly IR-driven product CHIRPS struggles in these departments. The analysis of the IMERG products shows a gradual improvement in skill from the Early to the Final Run (IMERG-E vs IMERG-F) and from the old to the new version (IMERG-F vs IMERG-V7).
- There is an evident seasonal cycle in performance where the products behave best (worst) in austral winter (summer), suggesting improved performance when rainfall is

more frequently driven by synoptic-scale weather patterns in JJA. Furthermore, there are indications that skill decreases toward the central part of the domain.

- None of the products are skillful in the estimation of observed extreme values (i.e., >95th percentile) with the Nash–Sutcliffe coefficient being all negative. False alarms are also prevalent across all precipitation products, suggesting considerable challenges in the perceptivity and handling of extreme rainfall. The analysis with Taylor and QQ diagrams highlights the tendency of strong underestimation by all products, but it is least pronounced in CHIRPS.
- The frequency of low-intensity precipitation is overestimated by all products but least by CHIRPS. Sampling for coinciding wet days only between observation and test data (i.e., hits) shows an improvement for ERA5 and MSWEP, suggesting a superior treatment of weak to moderate rainfall.
- Taking the arithmetic mean of successively more stations in a pixel as reference data leads to an overall performance improvement with all SPPs, highlighting the deficiencies of the often criticized but inevitable point-to-pixel comparison approach. However, the key characteristics of the SPPs listed above remain.

In the context of multi-SPP validation work across the African continent, the body of literature for southern Africa, and South Africa in particular, is considerably smaller than for the tropical and more convection-driven rainfall regimes of West, central, and East Africa. Nonetheless, a common finding between this and many other African study regions, especially East Africa, is the difficulty of skillful precipitation estimation over complex terrain (Dinku et al. 2008; Thiemig et al. 2012; Monsieurs et al. 2018) which has largely been attributed to warm orographic rain processes (Dinku et al. 2011; Diem et al. 2014; Cattani et al. 2021). Indeed, at some stations along mountain lines like De Doorns (3), Fizantekraal (7), and Rouxpos (19), all SPPs exhibit a lower HSS than the respective mean value (not shown), hinting toward similar challenges in the Western Cape region. As corroborated by, e.g., Yamamoto et al. (2017), both IR- and PMW-based products tend to underestimate or even miss warm rain processes in shallow orographic clouds due to limitations in their respective rainfall retrieval schemes, i.e., the reliance on low cloud-top temperatures and cloud-ice scattering, respectively. Furthermore, difficulties in capturing high-percentile rainfall are in line with comparative studies across Africa (Ali et al. 2005; Thiemig et al. 2012, Dembélé and Zwart 2016; Le Coz and van de Giesen 2020). This is partially inflicted by the point-to-pixel comparison approach, for which this study showed that a slight improvement is made if successively more stations are considered within a pixel. These limitations inhibit the use of SPP data in hydrological applications and monitoring in the Western Cape where high rainfalls in mountainous regions drive streamflows and affect dam storage. A number of these crucial stations/locations (Jonkershoek, Nuweberg—in the headwaters of major reservoirs) had low-performance metrics, while other less-important stations in terms of hydrological diversity had higher performance (Strand). Additionally, none of the SPPs attained good performance for the 95th percentile, and performance was reduced during the dry season (DJF). While the use of these SPPs may be limited for estimating/evaluating flood event rainfalls, SPPs, particularly ERA5 and MSWEP, show great potential for daily monitoring and for general meteorological patterns to still be captured. Further improvements are still needed to SPPs for their use to capture precipitation extremes.

The ranking in the skill of the SPPs, with the reanalysis-driven products ERA5 and MSWEP performing best, is the most striking difference between the Mediterranean climate of the Western Cape Province and the largely convective setting of the tropical regions. It has been widely shown that PMW-based products, especially those merged with IR and station information, can outperform other (e.g., IR-focused or reanalysis) datasets on a daily time scale (e.g., Roca et al. 2010; Bitew and Gebremichael 2011; Thiemig et al. 2012; Dembélé and Zwart 2016; Serrat-Capdevila et al. 2016; Camberlin et al. 2019; Satgé et al. 2020; Ageet et al. 2022), even though it is stressed that the general skill of SPPs can be low. Rainfall in the Western Cape of South Africa is frequently caused by frontal passages (Cattani et al. 2021; Du Plessis and Kibii 2021) in conjunction with synoptic-scale weather patterns. As these patterns are resolved by global models, rainfall estimations from reanalysis data arguably exhibit higher usability than in equatorial Africa (cf. Maidment et al. 2013), even though the wet-day frequency is by far the highest for both ERA5 and MSWEP (not shown). Beyond this, the more extratropical rainfall regime of the Western Cape Province likely imposes a more pronounced challenge for IR-based products like CHIRPS compared to the tropics. In an in-depth intercomparison SPP study for southern Africa including CHIRPS, MSWEP, and TAMSAT, Cattani et al. (2021) highlight difficulties in rainfall estimation in coastal and mountainous areas due to cloud systems with CTTs potentially higher than the detection threshold in the algorithms. The poor distinction between wet and dry days by CHIRPS, consequently, is also noted by Maswanganye (2018).

In conclusion, precipitation data scarcity plagues much of Africa, South America, and Asia, impacting water resource planning and the ability to develop hydrological models to prepare for inevitable climate extremes and variability. Satellite-based precipitation products (SPPs) are globally available at good spatial and temporal resolution, but inaccuracies impact hydrological model performance, parameter uncertainty, and the ability to simulate peak, low flows, and hydrological seasonality. ERA5 and MSWEP are the best-performing SPPs for the Mediterranean Western Cape with the best Heidke skill score, bias in detection, and probability of detection. SPPs are, however, not recommended for use in flood simulation and drought modeling in the Western Cape region given the low 95th percentile and dry season (DJF) performance. SPP performance is more related to climate type as opposed to altitude, and therefore, future improvements in SPPs should focus on local microclimatic variability and capturing headwater precipitation patterns. Future research is required to identify the location of a season-dependent latitude at which reanalysis products become inferior to PMW products. Further analysis

should also focus on the relative performance of these SPPs in their native resolutions as opposed to using a standard grid.

Acknowledgments. The authors acknowledge and thank the South African Weather Services and Agricultural Research Council for access to their observed rainfall data, without which this analysis would not be possible. AHF, MM, and JH acknowledge support from the Bundesministerium für Bildung und Forschung Grant 02WAS1713A "Co-design of a hydrometeorological information system for sustainable water resources management in southern Africa (CO-Hydim-SA)." The authors also thank the reviewers for their insight and valuable contributions, which improved the manuscript markedly.

Data availability statement. Due to its proprietary nature, supporting data cannot be made openly available. Further information about the data and conditions for access is available from the South African Weather Services or the Agricultural Research Council.

APPENDIX

Additional Analyses at SPP Native Resolutions

The appendix presents the results of the validation statistics conducted for the study at SPP native resolutions (as opposed to the common 0.25° grid results). Figure A1 displays the validation statistics of the various SPPs at their native resoution. Figure A2 reports the validation metrics by season at native resolutions. Table A1 presents the percentage of annual predicted rainfall at native resolutions, Table A2 provides the validation statistics for each SPP, and Table A3 gives the percentages of wet days (i.e., daily rainfall amount $\geq$ 0.2 mm) within the RGs and all SPPs over the study period 2012–21.

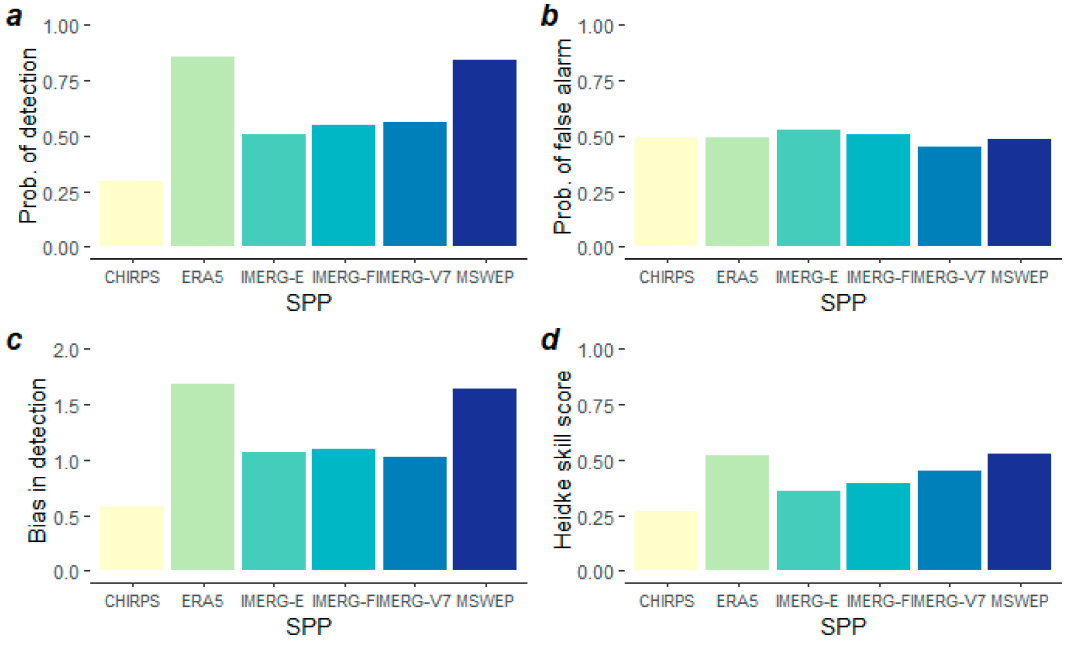

FIG. A1. Validation statistics at native resolutions (a) POD, (b) POFA, (c) BID, and (d) HSS.

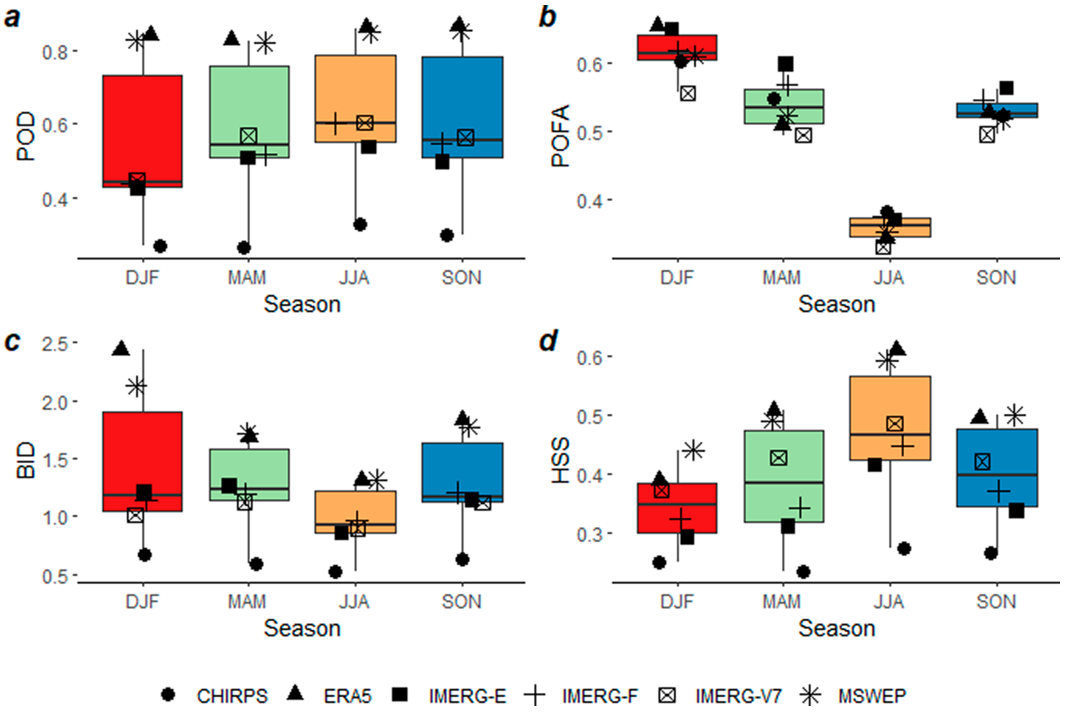

FIG. A2. Seasonal validation metrics at native resolutions.

TABLE A1. Percentage of annual predicted rainfall at native resolutions.

ID	Station	CHIRPS	ERA5	IMERG_E	IMERG_F	IMERGV7	MSWEP	Mean
1	Bokveldkloof	0.79	0.83	0.43	0.59	0.44	0.60	0.61
2	Ceres	0.44	0.47	0.24	0.37	0.30	0.40	0.37
3	De Doorns	0.91	1.32	0.87	1.25	1.02	1.23	1.10
4	Die Erf	1.02	1.26	0.77	1.10	0.82	1.04	1.00
5	Excelsior (Ceres)	0.89	1.03	0.74	0.92	0.74	0.91	0.87
6	Fishhoek	0.82	1.00	0.64	1.06	1.17	0.85	0.92
7	Fizantekraal	1.08	1.11	0.49	0.78	0.78	0.99	0.87
8	Helderberg Nature Reserve	0.86	0.89	0.46	0.72	0.77	0.81	0.75
9	Hoeko	0.94	0.82	0.94	0.87	0.90	0.85	0.89
10	Jan De Boers	1.01	1.03	1.24	1.28	1.20	0.99	1.12
11	Jonkershoek	0.71	0.68	0.29	0.49	0.53	0.69	0.56
12	Kirstenbosch	0.45	0.43	0.28	0.45	0.49	0.39	0.42
13	Klondyke	0.66	0.84	0.52	0.73	0.60	0.72	0.68
14	Molteno Reservoir	0.81	0.86	0.56	0.92	0.99	0.80	0.82
15	Murraysberg	0.63	0.88	1.55	0.87	0.86	0.83	0.94
16	Nuweberg	0.62	0.56	0.27	0.44	0.46	0.56	0.49
17	Oudebosch	0.52	0.55	0.39	0.58	0.63	0.57	0.54
18	Robertson	1.05	1.21	0.78	1.07	1.09	1.15	1.06
19	Rouxpos	1.59	0.97	1.09	1.07	1.16	0.96	1.14
20	Strand	NA	1.01	0.66	1.02	1.11	1.04	0.97
21	Welbedacht	1.04	1.15	0.45	0.74	0.77	0.98	0.85
22	Zuurvlakte	0.40	0.53	0.22	0.32	0.30	0.41	0.36
	Mean	0.82	0.88	0.63	0.80	0.78	0.81	0.79

TABLE A2. Validation statistics at native resolutions.

SPP	POD	POFA	BID	HSS	*r*	MAE	PB	RMSE	*E*
CHIRPS	0.30	0.49	0.58	0.27	0.23	9.09	−0.65	17.47	−0.35
ERA5	0.85	0.49	1.68	0.52	0.57	6.10	−0.84	12.69	0.26
IMERG-E	0.50	0.53	1.06	0.36	0.31	8.29	−0.17	15.66	−0.13
IMERG-F	0.55	0.50	1.09	0.40	0.46	7.57	−0.36	14.26	0.06
IMERG-V7	0.56	0.45	1.02	0.45	0.47	7.41	−0.41	14.12	0.08
MSWEP	0.84	0.48	1.63	0.52	0.55	6.23	−0.71	12.90	0.23
					Extremes				
CHIRPS					0.08	44.72	0.73	54.98	−2.29
ERA5					0.16	32.51	0.56	44.06	−1.19
IMERG-E					0.01	39.90	0.68	50.31	−1.86
IMERG-F					0.09	32.82	0.45	44.46	−1.26
IMERG-V7					0.10	33.90	0.50	45.52	−1.34
MSWEP					0.17	33.64	0.59	45.10	−1.24

TABLE A3. Percentages of wet days (i.e., daily rainfall amount ≥ 0.2 mm) within the RGs and all SPPs over the study period 2012–21. Only days for which rainfall data across all products are available are sampled.

SPP	RGs	CHIRPS	ERA5	IMERG-E	IMERG-F	IMERG-V7	MSWEP
Percent of wet days	21.7	26.5	38.2	26.3	26.8	26.6	35.2

REFERENCES

Adler, R. F., and Coauthors, 2003: The version-2 Global Precipitation Climatology Project (GPCP) monthly precipitation analysis (1979–present). *J. Hydrometeor.*, **4**, 1147–1167, https://doi.org/10.1175/1525-7541(2003)004<1147:TVGPCP>2.0.CO;2.

Ageet, S., A. H. Fink, M. Maranan, J. E. Diem, J. Hartter, A. L. Ssali, and P. Ayabagabo, 2022: Validation of satellite rainfall estimates over equatorial East Africa. *J. Hydrometeor.*, **23**, 129–151, https://doi.org/10.1175/JHM-D-21-0145.1.

Ali, A., A. Amani, A. Diedhiou, and T. Lebel, 2005: Rainfall estimation in the Sahel. Part II: Evaluation of rain gauge networks in the CILSS countries and objective intercomparison of rainfall products. *J. Appl. Meteor.*, **44**, 1707–1722, https://doi.org/10.1175/JAM2305.1.

Arkin, P. A., and B. N. Meisner, 1987: The relationship between large-scale convective rainfall and cold cloud over the western hemisphere during 1982–84. *Mon. Wea. Rev.*, **115**, 51–74, https://doi.org/10.1175/1520-0493(1987)115<0051:TRBLSC>2.0.CO;2.

——, R. Joyce, and J. E. Janowiak, 1994: The estimation of global monthly mean rainfall using infrared satellite data: The GOES precipitation index (GPI). *Remote Sens. Rev.*, **11**, 107–124, https://doi.org/10.1080/02757259409532261.

Awange, J. L., V. G. Ferreira, E. Forootan, S. A. Andam-Akorful, N. O. Agutu, and X. F. He, 2016: Uncertainties in remotely sensed precipitation data over Africa. *Int. J. Climatol.*, **36**, 303–323, https://doi.org/10.1002/joc.4346.

Bailey, A. K., and W. V. Pitman, 2015: Water Resources of South Africa, 2012 Study (WR2012). Water Research Commission Rep. K5/2143/1 (Issue 2143/1), 161 pp., https://waterresourceswr2012.co.za/.

Beck, H. E., A. I. J. M. van Dijk, V. Levizzani, J. Schellekens, D. G. Miralles, B. Martens, and A. de Roo, 2017: MSWEP: 3-hourly 0.25° global gridded precipitation (1979–2015) by merging gauge, satellite, and reanalysis data. *Hydrol. Earth Syst. Sci.*, **21**, 589–615, https://doi.org/10.5194/hess-21-589-2017.

——, and Coauthors, 2019: Daily evaluation of 26 precipitation datasets using Stage-IV gauge-radar data for the CONUS. *Hydrol. Earth Syst. Sci.*, **23**, 207–224, https://doi.org/10.5194/hess-23-207-2019.

Bitew, M. M., and M. Gebremichael, 2011: Assessment of satellite rainfall products for streamflow simulation in medium watersheds of the Ethiopian highlands. *Hydrol. Earth Syst. Sci.*, **15**, 1147–1155, https://doi.org/10.5194/hess-15-1147-2011.

Brunner, M. I., L. Slater, L. M. Tallaksen, and M. Clark, 2021: Challenges in modeling and predicting floods and droughts: A review. *Wiley Interdiscip. Rev.: Water*, **8**, e1520, https://doi.org/10.1002/wat2.1520.

Bulovic, N., N. Mcintyre, and F. Johnson, 2020: Evaluation of IMERG V05B 30-min rainfall estimates over the high-elevation tropical Andes Mountains. *J. Hydrometeor.*, **21**, 2875–2892, https://doi.org/10.1175/JHM-D-20-0114.1.

Calvo-Solano, O., and A. Quesada-Román, 2024: Worldwide research trends and networks on flood early warning systems. *GeoHazards*, **5**, 582–595, https://doi.org/10.3390/geohazards5030030.

Camberlin, P., and Coauthors, 2019: Evaluation of remotely sensed rainfall products over Central Africa. *Quart. J. Roy. Meteor. Soc.*, **145**, 2115–2138, https://doi.org/10.1002/qj.3547.

Cattani, E., O. Ferguglia, A. Merino, and V. Levizzani, 2021: Precipitation products' inter–comparison over East and southern Africa 1983–2017. *Remote Sens.*, **13**, 4419, https://doi.org/10.3390/rs13214419.

Chawla, I., and P. P. Mujumdar, 2020: Evaluating rainfall datasets to reconstruct floods in data-sparse Himalayan region. *J. Hydrol.*, **588**, 125090, https://doi.org/10.1016/j.jhydrol.2020.125090.

Cohen Liechti, T., J. P. Matos, J.-L. Boillat, and A. J. Schleiss, 2012: Comparison and evaluation of satellite derived precipitation products for hydrological modeling of the Zambezi River Basin. *Hydrol. Earth Syst. Sci.*, **16**, 489–500, https://doi.org/10.5194/hess-16-489-2012.

Copernicus, 2023: ERA5 hourly data on single levels from 1940 to present. Accessed 7 July 2023, https://cds.climate.copernicus.eu/cdsapp#!/dataset/reanalysis-era5-single-levels?tab=doc.

Craig, H., 1961: Isotopic variations in meteoric waters. *Science*, **133**, 1702–1703, https://doi.org/10.1126/science.133.3465.1702.

Council for Scientific and Industrial Research, 2015: Climate indicators: Köppen-Geiger climate classification. Accessed 13 January 2025, https://stepsatest.csir.co.za/climate_koppen_geiger.html.

De Coning, E., 2013: Optimizing satellite-based precipitation estimation for nowcasting of rainfall and flash flood events over the South African domain. *Remote Sens.*, **5**, 5702–5724, https://doi.org/10.3390/rs5115702.

——, and E. Poolman, 2011: South African Weather Service operational satellite based precipitation estimation technique: Applications and improvements. *Hydrol. Earth Syst. Sci.*, **15**, 1131–1145, https://doi.org/10.5194/hess-15-1131-2011.

Dembélé, M., and S. J. Zwart, 2016: Evaluation and comparison of satellite-based rainfall products in Burkina Faso, West Africa. *Int. J. Remote Sens.*, **37**, 3995–4014, https://doi.org/10.1080/01431161.2016.1207258.

de Waal, J. H., A. Chapman, and J. Kemp, 2017: Extreme 1-day rainfall distributions: Analysing change in the Western Cape. *S. Afr. J. Sci.*, **113**, 8, https://doi.org/10.17159/sajs.2017/20160301.

de Waal, J., J. Miller, and A. van Niekerk, 2023: The impact of agricultural transformation on water quality in a data-scarce, dryland landscape—A case study in the Bot River, South Africa. *Environ. Monitoring Assess.*, **195**, 177, https://doi.org/10.1007/s10661-022-10776-4.

Diem, J. E., J. Hartter, S. J. Ryan, and W. M. Palace, 2014: Validation of satellite rainfall products for western Uganda. *J. Hydrometeor.*, **15**, 2030–2038, https://doi.org/10.1175/JHM-D-13-0193.1.

Dinku, T., S. Chidzambwa, P. Ceccato, S. J. Connor, and C. F. Ropelewski, 2008: Validation of high-resolution satellite rainfall products over complex terrain. *Int. J. Remote Sens.*, **29**, 4097–4110, https://doi.org/10.1080/01431160701772526.

——, P. Ceccato, and S. J. Connor, 2011: Challenges of satellite rainfall estimation over mountainous and arid parts of East Africa. *Int. J. Remote Sens.*, **32**, 5965–5979, https://doi.org/10.1080/01431161.2010.499381.

Du Plessis, J. A., and B. Schloms, 2017: An investigation into the evidence of seasonal rainfall pattern shifts in the Western Cape, South Africa. *J. S. Afr. Inst. Civil Eng.*, **59**, 47–55, https://doi.org/10.17159/2309-8775/2017/v59n4a5.

——, and J. K. Kibii, 2021: Applicability of CHIRPS-based satellite rainfall estimates for South Africa. *J. S. Afr. Inst. Civil Eng.*, **63**, 43–54, https://doi.org/10.17159/2309-8775/2021/v63n3a4.

Funk, C., and Coauthors, 2015: The climate hazards infrared precipitation with stations—A new environmental record for monitoring extremes. *Sci. Data*, **2**, 150066, https://doi.org/10.1038/sdata.2015.66.

Geleta, C. D., and T. A. Deressa, 2021: Evaluation of Climate Hazards Group InfraRed Precipitation Station (CHIRPS) satellite-based rainfall estimates over Finchaa and Neshe watersheds, Ethiopia. *Eng. Rep.*, **3**, e12338, https://doi.org/10.1002/eng2.12338.

Hanke, M., R. Redler, T. Holfeld, and M. Yastremsky, 2016: YAC 1.2.0: New aspects for coupling software in Earth system modelling. *Geosci. Model Dev.*, **9**, 2755–2769, https://doi.org/10.5194/gmd-9-2755-2016.

Harris, C., C. Burgers, J. Miller, and F. Rawoot, 2010: O- and H-isotope record of Cape Town rainfall from 1996 to 2008, and its application to recharge studies of Table Mountain groundwater, South Africa. *S. Afr. J. Geol.*, **113**, 33–56, https://doi.org/10.2113/gssajg.113.1.33.

Hersbach, H., and Coauthors, 2020: The ERA5 global reanalysis. *Quart. J. Roy. Meteor. Soc.*, **146**, 1999–2049, https://doi.org/10.1002/qj.3803.

Holloway, A., G. Fortune, P. Zweig, L. Barrett, A. Benjamin, V. Chasi, and J. de Waal, 2012: Eden and Central Karoo Drought Disaster 2009–2011: "The Scramble for Water". Disaster Mitigation for Sustainable Livelihoods Programme, 132 pp., https://d7.westerncape.gov.za/sites/www.westerncape.gov.za/files/documents/2012/11/eden-and-central-karoo-drought-disaster-2009-2011.pdf.

Hou, A. Y., and Coauthors, 2014: The Global Precipitation Measurement mission. *Bull. Amer. Meteor. Soc.*, **95**, 701–722, https://doi.org/10.1175/BAMS-D-13-00164.1.

Hsu, K.-L., X. Gao, S. Sorooshian, and H. V. Gupta, 1997: Precipitation estimation from remotely sensed information using artificial neural networks. *J. Appl. Meteor.*, **36**, 1176–1190, https://doi.org/10.1175/1520-0450(1997)036<1176:PEFRSI>2.0.CO;2.

Huffman, G. J., and Coauthors, 1997: The Global Precipitation Climatology Project (GPCP) combined precipitation dataset. *Bull. Amer. Meteor. Soc.*, **78**, 5–20, https://doi.org/10.1175/1520-0477(1997)078<0005:TGPCPG>2.0.CO;2.

——, and Coauthors, 2007: The TRMM Multisatellite Precipitation Analysis (TMPA): Quasi-global, multiyear, combined-sensor precipitation estimates at fine scales. *J. Hydrometeor.*, **8**, 38–55, https://doi.org/10.1175/JHM560.1.

——, R. F. Adler, D. T. Bolvin, and E. J. Nelkin, 2010: The TRMM multi-satellite precipitation analysis (TMPA). *Satellite Rainfall Applications for Surface Hydrology*, M. Gebremichael and F. Hossain, Eds., Springer, 3–22, https://doi.org/10.1007/978-90-481-2915-7_1.

——, D. T. Bolvin, and E. J. Nelkin, 2017: Integrated Multi-satellite retrievals for GPM (IMERG) technical documentation. NASA Tech. Doc., 54 pp., https://pmm.nasa.gov/sites/default/files/document_files/IMERG_technical_doc_3_22_17.pdf.

Hughes, D. A., 2006: Comparison of satellite rainfall data with observations from gauging station networks. *J. Hydrol.*, **327**, 399–410, https://doi.org/10.1016/j.jhydrol.2005.11.041.

Joyce, R. J., J. E. Janowiak, P. A. Arkin, and P. Xie, 2004: CMORPH: A method that produces global precipitation estimates from passive microwave and infrared data at high spatial and temporal resolution. *J. Hydrometeor.*, **5**, 487–503, https://doi.org/10.1175/1525-7541(2004)005<0487:CAMTPG>2.0.CO;2.

Kidd, C., and V. Levizzani, 2011: Status of satellite precipitation retrievals. *Hydrol. Earth Syst. Sci.*, **15**, 1109–1116, https://doi.org/10.5194/hess-15-1109-2011.

Kimani, M. W., J. C. B. Hoedjes, and Z. Su, 2017: An assessment of satellite-derived rainfall products relative to ground observations over East Africa. *Remote Sens.*, **9**, 430, https://doi.org/10.3390/rs9050430.

Kreibich, H., and Coauthors, 2022: The challenge of unprecedented floods and droughts in risk management. *Nature*, **608**, 80–86, https://doi.org/10.1038/s41586-022-04917-5.

Kubota, T., and Coauthors, 2007: Global precipitation map using satellite-borne microwave radiometers by the GSMaP project: Production and validation. *IEEE Trans. Geosci. Remote Sens.*, **45**, 2259–2275, https://doi.org/10.1109/TGRS.2007.895337.

Kummerow, C., and Coauthors, 2000: The status of the Tropical Rainfall Measuring Mission (TRMM) after two years in orbit. *J. Appl. Meteor.*, **39**, 1965–1982, https://doi.org/10.1175/1520-0450(2001)040<1965:TSOTTR>2.0.CO;2.

Lakew, H. B., S. A. Moges, and D. H. Asfaw, 2020: Hydrological performance evaluation of multiple satellite precipitation products in the upper Blue Nile basin, Ethiopia. *J. Hydrol. Reg. Stud.*, **27**, 100664, https://doi.org/10.1016/j.ejrh.2020.100664.

Lavers, D. A., A. Simmons, F. Vamborg, and M. J. Rodwell, 2022: An evaluation of ERA5 precipitation for climate monitoring. *Quart. J. Roy. Meteor. Soc.*, **148**, 3152–3165, https://doi.org/10.1002/qj.4351.

Le Coz, C., and N. van de Giesen, 2020: Comparison of rainfall products over sub-Saharan Africa. *J. Hydrometeor.*, **21**, 553–596, https://doi.org/10.1175/JHM-D-18-0256.1.

Maidment, R. I., D. I. F. Grimes, R. P. Allan, H. Greatrex, O. Rojas, and O. Leo, 2013: Evaluation of satellite-based and model re-analysis rainfall estimates for Uganda. *Meteor. Appl.*, **20**, 308–317, https://doi.org/10.1002/met.1283.

——, D. Grimes, R. P. Allan, E. Tarnavsky, M. Stringer, T. Hewison, R. Roebeling, and E. Black, 2014: The 30 year TAMSAT African Rainfall Climatology and Time Series (TARCAT) data set. *J. Geophys. Res. Atmos.*, **119**, 10 619–10 644, https://doi.org/10.1002/2014JD021927.

Mal, S., R. B. Singh, C. Huggel, and A. Grover, 2018: Introducing linkages between climate change, extreme events, and disaster risk reduction. *Climate Change, Extreme Events and Disaster Risk Reduction*, S. Mal, R. Singh, and C. Huggel, Eds., Sustainable Development Goals Series, Springer, 1–14, https://doi.org/10.1007/978-3-319-56469-2_1.

Maranan, M., A. H. Fink, P. Knippertz, L. K. Amekudzi, W. A. Atiah, and M. Stengel, 2020: A process-based validation of GPM IMERG and its sources using a mesoscale rain gauge network in the West African forest zone. *J. Hydrometeor.*, **21**, 729–749, https://doi.org/10.1175/JHM-D-19-0257.1.

Maswanganye, S. E., 2018: A comparison of remotely-sensed precipitation estimates with observed data from rain gauges in the Western Cape, South Africa. M.S. Thesis, Dept. of Earth Science, University of the Western Cape, 121 pp., https://www.researchgate.net/publication/367339836_A_COMPARISON_OF_REMOTELY-SENSED_PRECIPITATION_ESTIMATES_WITH_OBSERVED_DATA_FROM_RAIN_GAUGES_IN_THE_WESTERN_CAPE_SOUTH_AFRICA.

McCollum, J. R., A. Gruber, and M. B. Ba, 2000: Discrepancy between gauges and satellite estimates of rainfall in equatorial Africa. *J. Appl. Meteor.*, **39**, 666–679, https://doi.org/10.1175/1520-0450-39.5.666.

Monsieurs, E., and Coauthors, 2018: Evaluating TMPA rainfall over the sparsely gauged East African Rift. *J. Hydrometeor.*, **19**, 1507–1528, https://doi.org/10.1175/JHM-D-18-0103.1.

NASA, 2023: The Global Precipitation Measurement Mission (GPM). Accessed 7 July 2023, https://gpm.nasa.gov/missions/GPM.

Nguyen, P., M. Ombadi, S. Sorooshian, K. Hsu, A. AghaKouchak, D. Braithwaite, H. Ashouri, and A. R. Thorstensen, 2018: The PERSIANN family of global satellite precipitation data: A review and evaluation of products. *Hydrol. Earth Syst. Sci.*, **22**, 5801–5816, https://doi.org/10.5194/hess-22-5801-2018.

Nicholson, S. E., and Coauthors, 2003: Validation of TRMM and other rainfall estimates with a high-density gauge dataset for West Africa. Part I: Validation of GPCC rainfall product and pre-TRMM satellite and blended products. *J. Appl. Meteor.*, **42**, 1337–1354, https://doi.org/10.1175/1520-0450(2003)042<1337:VOTAOR>2.0.CO;2.

——, C. Funk, and A. H. Fink, 2018a: Rainfall over the African continent from the 19th through the 21st century. *Global Planet. Change*, **165**, 114–127, https://doi.org/10.1016/j.gloplacha.2017.12.014.

——, A. H. Fink, and C. Funk, 2018b: Assessing recovery and change in West Africa's rainfall regime from a 161-year record. *Int. J. Climatol.*, **38**, 3770–3786, https://doi.org/10.1002/joc.5530.

Preston-Whyte, R. A., and P. D. Tyson, 1988: *The Atmosphere and Weather of Southern Africa.* Oxford University Press, 374 pp.

Roberts, N., M. E. Meadows, and J. R. Dodson, 2001: The history of Mediterranean-type environments: Climate, culture and landscape. *Holocene*, **11**, 631–634, https://doi.org/10.1191/09596830195663.

Roca, R., P. Chambon, I. Jobard, P.-M. Kirstetter, M. Gosset, and J. C. Bergès, 2010: Comparing satellite and surface rainfall products over West Africa at meteorologically relevant scales during the AMMA campaign using error estimates. *J. Appl. Meteor. Climatol.*, **49**, 715–731, https://doi.org/10.1175/2009JAMC2318.1.

Romilly, T. G., and M. Gebremichael, 2011: Evaluation of satellite rainfall estimates over Ethiopian river basins. *Hydrol. Earth Syst. Sci.*, **15**, 1505–1514, https://doi.org/10.5194/hess-15-1505-2011.

Satgé, F., D. Defrance, B. Sultan, M.-P. Bonnet, F. Seyler, N. Rouché, F. Pierron, and J.-E. Paturel, 2020: Evaluation of 23 gridded precipitation datasets across West Africa. *J. Hydrol.*, **581**, 124412, https://doi.org/10.1016/j.jhydrol.2019.124412.

Sawunyama, T., and D. A. Hughes, 2008: Application of satellite-derived rainfall estimates to extend water resource simulation modelling in South Africa. *Water S. Afr.*, **34**, 1–10, https://doi.org/10.4314/wsa.v34i1.180739.

Schneider, U., T. Fuchs, A. Meyer-Christoffer, and B. Rudolf, 2008: Global precipitation analysis products of the GPCC. *Global Precipitation Climatology Centre (GPCC)*, DWD, Internet Publikation, 3819–3837.

Schulzweida, U., 2023: CDO user guide 2.3.0. Zenodo, accessed 01 February 2024, https://doi.org/10.5281/zenodo.10020800.

Serrat-Capdevila, A., M. Merino, J. B. Valdes, and M. Durcik, 2016: Evaluation of the performance of three satellite precipitation products over Africa. *Remote Sens.*, **8**, 836, https://doi.org/10.3390/rs8100836.

Sun, G., Y. Wei, G. Wang, R. Shi, H. Chen, and C. Mo, 2022: Downscaling correction and hydrological applicability of the three latest high-resolution satellite precipitation products (GPM, GSMAP, and MSWEP) in the Pingtang catchment, China. *Adv. Meteor.*, **2022**, 6507109, https://doi.org/10.1155/2022/6507109.

Tan, J., W. A. Petersen, and A. Tokay, 2016: A novel approach to identify sources of errors in IMERG for GPM ground validation. *J. Hydrometeor.*, **17**, 2477–2491, https://doi.org/10.1175/JHM-D-16-0079.1.

——, G. J. Huffman, D. T. Bolvin, E. J. Nelkin, and M. Rajagopal, 2021: SHARPEN: A scheme to restore the distribution of averaged precipitation fields. *J. Hydrometeor.*, **22**, 2105–2116, https://doi.org/10.1175/JHM-D-20-0225.1.

Tapiador, F. J., A. Navarro, R. Martín, S. Hristova-Veleva, and Z. S. Haddad, 2022: Predicting tropical cyclone rapid intensification from satellite microwave data and neural networks. *IEEE Trans. Geosci. Remote Sens.*, **60**, 4205213, https://doi.org/10.1109/TGRS.2021.3128076.

Tarnavsky, E., D. Grimes, R. Maidment, E. Black, R. P. Allan, M. Stringer, R. Chadwick, and F. Kayitakire, 2014: Extension of the TAMSAT satellite-based rainfall monitoring over Africa and from 1983 to present. *J. Appl. Meteor. Climatol.*, **53**, 2805–2822, https://doi.org/10.1175/JAMC-D-14-0016.1.

Taylor, K. E., 2001: Summarizing multiple aspects of model performance in a single diagram. *J. Geophys. Res.*, **106**, 7183–7192, https://doi.org/10.1029/2000JD900719.

——, 2024: Truly conserving with conservative remapping methods. *Geosci. Model Dev.*, **17**, 415–430, https://doi.org/10.5194/gmd-17-415-2024.

Thiemig, V., R. Rojas, M. Zambrano-Bigiarini, V. Levizzani, and A. De Roo, 2012: Validation of satellite-based precipitation products over sparsely gauged African river basins. *J. Hydrometeor.*, **13**, 1760–1783, https://doi.org/10.1175/JHM-D-12-032.1.

Toté, C., D. Patricio, H. Boogaard, R. Van der Wijngaart, E. Tarnavsky, and C. Funk, 2015: Evaluation of satellite rainfall estimates for drought and flood monitoring in Mozambique. *Remote Sens.*, **7**, 1758–1776, https://doi.org/10.3390/rs70201758.

Ushio, T., and Coauthors, 2003: The Global Satellite Mapping of Precipitation (GSMaP) project. Aqua (AMSR-E), 2004, 2 pp.

Villarini, G., P. V. Mandapaka, W. F. Krajewski, and R. J. Moore, 2008: Rainfall and sampling uncertainties: A rain gauge perspective. *J. Geophys. Res.*, **113**, D11102, https://doi.org/10.1029/2007JD009214.

Washington, R., and Coauthors, 2006: African climate change: Taking the shorter route. *Bull. Amer. Meteor. Soc.*, **87**, 1355–1366, https://doi.org/10.1175/BAMS-87-10-1355.

Western Cape Government, 2024: Roads storm damage report - July and August 2024. Accessed 5 December 2024, https://www.westerncape.gov.za/department-of-infrastructure/roads-storm-damage-report-july-and-august-2024.

Wolski, P., 2018: How severe is Cape Town's "day zero" drought? *Significance*, **15**, 24–27, https://doi.org/10.1111/j.1740-9713.2018.01127.x.

Yamamoto, M. K., S. Shige, C.-K. Yu, and L.-W. Cheng, 2017: Further improvement of the heavy orographic rainfall retrievals in the GSMaP algorithm for microwave radiometers. *J. Appl. Meteor. Climatol.*, **56**, 2607–2619, https://doi.org/10.1175/JAMC-D-16-0332.1.

Yang, T.-H., and W.-C. Liu, 2020: A general overview of the risk-reduction strategies for floods and droughts. *Sustainability*, **12**, 2687, https://doi.org/10.3390/su12072687.

Ward, P. J., and Coauthors, 2020: The need to integrate flood and drought disaster risk reduction strategies. *Water Secur.*, **11**, 100070, https://doi.org/10.1016/j.wasec.2020.100070.

Zeng, Q., H. Chen, C.-Y. Xu, M.-X. Jie, J. Chen, S.-L. Guo, and J. Liu, 2018: The effect of rain gauge density and distribution on runoff simulation using a lumped hydrological modelling approach. *J. Hydrol.*, **563**, 106–122, https://doi.org/10.1016/j.jhydrol.2018.05.058.